

PREPARATION AND CHARACTERIZATION OF CARBON SUPPORTED  
PLATINUM NANOCATALYSTS WITH DIFFERENT SURFACTANTS FOR C1  
TO C3 ALCOHOL OXIDATIONS

A THESIS SUBMITTED TO  
THE GRADUATE SCHOOL OF NATURAL AND APPLIED SCIENCES  
OF  
MIDDLE EAST TECHNICAL UNIVERSITY

BY

SALİH ERTAN

IN PARTIAL FULFILLMENT OF THE REQUIREMENTS  
FOR  
THE DEGREE OF MASTER OF SCIENCE  
IN  
CHEMISTRY

SEPTEMBER 2011

Approval of the thesis:

**PREPARATION AND CHARACTERIZATION OF CARBON SUPPORTED  
PLATINUM NANOCATALYSTS WITH DIFFERENT SURFACTANTS FOR  
C1 TO C3 ALCOHOL OXIDATIONS**

submitted by **SALİH ERTAN** in partial fulfillment of the requirements for the degree of **Master of Science in Chemistry Department, Middle East Technical University** by,

Prof. Dr. Canan Özgen  
Dean, Graduate School of **Natural and Applied Sciences** \_\_\_\_\_

Prof. Dr. İlker Özkan  
Head of Department, **Chemistry** \_\_\_\_\_

Prof. Dr. Gülsün Gökağaç Arslan  
Supervisor, **Chemistry Department**, METU \_\_\_\_\_

**Examining Committee Members:**

Prof. Dr. İnci Eroğlu  
Chemical Engineering Dept., METU \_\_\_\_\_

Prof. Dr. Gülsün Gökağaç Arslan  
Chemistry Dept., METU \_\_\_\_\_

Assoc. Dr. Şeniz Özalp Yaman  
Chemical Eng. And Ap. Chemistry Dept., Atilim Uni. \_\_\_\_\_

Assoc. Prof. Dr. Ayşen Yılmaz  
Chemistry Dept., METU \_\_\_\_\_

Assist. Prof. Dr. Emren Nalbant Esentürk  
Chemistry Dept., METU \_\_\_\_\_

**Date:** 15/09/2011

**I hereby declare that all information in this document has been obtained and presented in accordance with academic rules and ethical conduct. I also declare that, as required by these rules and conduct, I have fully cited and referenced all materials and results that are not original to this work.**

Name, Last name: Salih Ertan

Signature:

## ABSTRACT

### PREPARATION AND CHARACTERIZATION OF CARBON SUPPORTED PLATINUM NANOCATALYSTS WITH DIFFERENT SURFACTANTS FOR C1 TO C3 ALCOHOL OXIDATIONS

Ertan, Salih

M. Sc., Department of Chemistry

Supervisor: Prof. Dr. Gülsün Gökağaç Arslan

September 2011, 46 pages

In this thesis, carbon supported platinum nanoparticles have been prepared by using  $\text{PtCl}_4$  as a starting material and 1-octanethiol, 1-decanethiol, 1-dodecanethiol and 1-hexadecanethiol as surfactants for methanol, ethanol and 2-propanol oxidation reactions. The structure, particle sizes and surface morphologies of the platinum were characterized by X-ray diffraction (XRD), atomic force microscopy (AFM) and transmission electron microscopy (TEM). XRD and TEM results indicate that all prepared catalysts have a face centered cubic structure and are homogeneously dispersed on the carbon support with a narrow size distribution (2.0 to 1.3 nm). X-ray photoelectron spectra of the catalysts were examined and it was found that platinum has two different oxidation state, Pt (0) and Pt (IV), oxygen and sulfur compounds are  $\text{H}_2\text{O}_{\text{ads}}$  and  $\text{OH}_{\text{ads}}$ , bounded and unbounded thiols. The electrochemical and electrocatalytic properties of those catalysts were investigated towards C1 to C3 alcohol oxidations by cyclic voltammetry (CV) and chronoamperometry (CA). The highest electrocatalytic activity was obtained from catalyst I which was prepared with 1-octanethiol. This may be attributed to decrease in the ratio of bounded to unbounded thiol species and increase in Pt (0)/Pt (IV),  $\text{H}_2\text{O}_{\text{ads}}/\text{OH}_{\text{ads}}$  ratios, electrochemical surface area, CO tolerance and percent platinum utility.

**Keywords:** Direct Methanol, Ethanol & 2-Propanol Fuel Cells, Carbon Supported Platinum Catalysts, Cyclic Voltammetry, Transmission Electron Microscopy, X-ray Photoelectron Spectroscopy, Atomic Force Microscopy.

## ÖZ

### C1'DEN C3'E KADAR OLAN ALKOL YÜKSELTGENME REAKSİYONLARI İÇİN KARBON DESTEKLİ PLATİN NANOKATALİZÖRLERİN HAZIRLANMASI VE KARAKTERİZASYONU

Ertan, Salih

Yüksek Lisans, Kimya Bölümü

Tez Yöneticisi: Prof. Dr. Gülsün Gökağaç Arslan

Eylül 2011, 46 sayfa

Bu çalışmada, metanol, etanol ve 2-propanol yükseltgenme tepkimeleri için karbon destekli platin nanoparçacıkları içeren katalizörler  $PtCl_4$  başlangıç maddesi ve 1-oktantiol, 1-dekantiol, 1-dodekantiol ve 1-hexadekantiol sürkatant olarak kullanılarak hazırlanmıştır. Platin metalinin yapısı, parçacık boyutları ve yüzey morfolojileri X-ışınları kırınımı, atomik kuvvet mikroskopi ve eşli geçirmeli elektron mikroskopi kullanılarak karakterize edilmiştir. XRD ve TEM sonuçları hazırlanan tüm katalizörlerde platinin yüzey merkezli kübik yapıya sahip olduğunu ve karbon desteğinin üzerinde dar boyut dağılımıyla homojen olarak yayıldığını göstermiştir (2.0' dan 1.3'e). Katalizörlerin X-ışını fotoelektron spektrumları incelenmiş ve platinin "0" ve "+4" olmak üzere iki değişik oksidasyon durumunda bulunduğunu, oksijen ve sülfür bileşiklerinin ise  $H_2O_{ads}$ ,  $OH_{ads}$ , yüzeye bağlı ve bağlı olmayan tioller şeklinde olduğu tespit edilmiştir. Bu katalizörlerin C1' den C3'e kadar alkollerin yükseltgenmesine karşı elektrokatalitik özellikleri dönüşümlü voltametre ve kronoamperometri ile incelenmiştir. En yüksek elektrokatalitik aktivite 1-oktantiol kullanılarak hazırlanan katalizörde gözlemlenmiştir. Bunun nedenlerinin yüzeye bağlı olan tiol/yüzeye bağlı olmayan tiol oranının düşük olmasının,  $Pt(0)/Pt(IV)$ ,  $H_2O_{ads}/OH_{ads}$  oranlarının, elektrokimya yüzey alanının, CO toleransının ve kullanılan platin yüzdesinin yüksek olmalarının olabileceği düşünülmüştür.

**Anahtar Kelimeler:** Doğrudan Metanol, Etanol ve 2-Propanol Yakıt Hücreleri, Karbon Destekli Platin Katalizörleri, Dönüşümlü Voltametre, Geçirmeli Elektron Mikroskobu, X-ışınları Fotoelektron Spektroskobu, Atomik Kuvvet Mikroskobu.

*To my parents and my wife,*

## ACKNOWLEDGEMENTS

I would like to thank to my advisor Prof. Dr. Glsn Gkaęa Arslan for giving me the opportunity to work in a well-equipped laboratory and on a challenging subject. Her recommendations and suggestions will always be guidance for my career.

I thank to Fatih Ően for his support, patience and belief in me during my study. He was/is always ready to answer my questions.

I want to thank to Selda Ően for her understanding and good friendship during my master years.

I owe many thanks to my lab partner Zafer ztrk who has no hesitation to help in any trouble.

I want to give my sincere thanks to Serdar Akbayrak for his warm friendship during my undergraduate and graduate years.

I want to express my gratitude to my friends, who were always with me in good time and in bad times.

I also want to thank to TUBITAK for supporting me financially in the project (108T065).

I thank to Atılım University for providing me a nice working environment.

I thank my parents for their love and support while I decided to be a “professional” student for awhile.

Finally, words alone cannot express the thanks that I owe to H. Glin zlu Ertan, my wife, for her love that touching my heart and making me a Don Quixote for every challenge in my life.

## TABLE OF CONTENTS

ABSTRACT.....	iv
ÖZ.....	vi
ACKNOWLEDGEMENTS.....	ix
TABLE OF CONTENTS.....	x
LIST OF TABLES.....	xii
LIST OF FIGURES.....	xiii
CHAPTERS.....	1
1. INTRODUCTION.....	1
1.1. THE CONCEPT OF FUEL CELL.....	1
1.2. THE BRIEF STORY OF FUEL CELL TECHNOLOGY.....	3
1.3. TYPES OF FUEL CELLS.....	6
1.4. DIRECT LIQUID FUEL CELLS.....	9
1.4.1. DIRECT METHANOL FUEL CELL.....	9
1.4.2. DIRECT ETHANOL FUEL CELL.....	12
1.4.3. DIRECT 2-PROPANOL FUEL CELL.....	13
1.5. THE CONCEPT OF NANOPARTICLE.....	14
1.6. THE AIM OF THE WORK.....	17
2. EXPERIMENTAL.....	19
2.1. SYNTHESIS OF CATALYSTS.....	19
2.1.1. SYNTHESIS OF THE CATALYST I.....	19
2.1.2. SYNTHESIS OF CATALYST II, III, IV.....	19
2.2. PREPARATION OF CARBON SUPPORTED PLATINUM CATALYST.....	20
2.3. PREPARATION OF ELECTRODE SOLUTION AND APPLICATION ON ELECTRODE.....	20
2.4. DETERMINATION OF PLATINUM CONTENT IN THE CATALYSTS.....	20
2.5. CHARACTERIZATION.....	21
2.5.1. CYCLIC VOLTAMMETRY (CV) AND CHRONOAMPEROMETRY (CA).....	21
2.5.2. X-RAY DIFFRACTION (XRD).....	21

2.5.3. TRANSMISSION ELECTRON MICROSCOPY (TEM) .....	21
2.5.4. X-RAY PHOTOELECTRON SPECTROSCOPY (XPS) .....	22
2.5.5. ATOMIC FORCE MICROSCOPY (AFM) .....	22
3. RESULTS AND DISCUSSION .....	23
3.1. X-RAY DIFFRACTION AND TRANSMISSION ELECTRON MICROSCOPY .....	23
3.2. X-RAY PHOTOELECTRON SPECTROSCOPY: .....	26
3.3. ATOMIC FORCE MICROSCOPY .....	30
3.4. CYCLIC VOLTAMMETRY .....	34
3.5. CHRONOAMPEROMETRY .....	41
4. CONCLUSIONS .....	42
REFERENCES .....	44

## LIST OF TABLES

### TABLES

<b>Table 1.1.</b> Types of fuel cells, their main properties and some applications. ....	8
<b>Table 2.1.</b> Platinum complexes and surfactant used for all the prepared catalysts. ..	20
<b>Table 3.1.</b> Pt 4f <sub>7/2</sub> core binding energies, eV, in the prepared catalysts. The number in the parentheses is the relative intensities of the species.....	28
<b>Table 3.2.</b> O 1s core binding energies, eV, in the prepared catalysts. (The numbers in the parentheses are the relative intensities of the species). ....	28
<b>Table 3.3.</b> S 2p <sub>3/2</sub> core binding energies, eV, in the prepared catalysts. (The number in the parentheses is the relative intensities of the species). ....	29
<b>Table 3.4.</b> Pt 4f and S 2p ratios determined by XPS. ....	29
<b>Table 3.5.</b> Average crystallite platinum particles size determined by (a) X-ray line broadening, (b) transmission electron microscopy, (c) particle height, (d) observed lateral diameter and (e) deconvoluted lateral diameter determined by AFM. ....	31
<b>Table 3.6.</b> Maximum currents, onset and anodic peak potentials and I <sub>f</sub> /I <sub>b</sub> ratios for all catalysts in MeOH, EtOH and 2-propanol. ....	38
<b>Table 3.7.</b> The comparison of particle size, ECSA/CSA (%Pt utility) for all catalyst. ....	40

## LIST OF FIGURES

### FIGURES

<b>Figure 1.1.</b> Grove's gas battery (1839). .....	4
<b>Figure 1.2.</b> Schematic representation of DMFC with solid acid electrolyte <sup>4</sup> .....	10
<b>Figure 1.3.</b> Formation of poisoning ( $\text{CO}_{\text{ads}}$ ) on the surface of the platinum. ....	11
<b>Figure 1.4.</b> Schematic representation of electrostatic stabilization. ....	15
<b>Figure 1.5.</b> Schematic representation of steric stabilization.....	16
<b>Figure 1.6.</b> Schematic representation of electrosteric stabilization.....	16
<b>Figure 1.7.</b> Schematic representation of ligand stabilization. ....	17
<b>Figure 3.1.</b> XRD of blank (a), catalyst I(c), II(d), III(e) and IV (b).....	24
<b>Figure 3.2.</b> High resolution transition electron micrograph and particle size histogram of a catalyst I. ....	25
<b>Figure 3.3.</b> Transmission electron micrograph of catalyst III. ....	26
<b>Figure 3.4.</b> Pt 4f electron spectra of catalyst I (a), II (b), III (c) and IV (d).....	27
<b>Figure 3.5.</b> AFM images of the catalysts. ....	31
<b>Figure 3.6.</b> Histogram of height of particles obtained from AFM data. ....	32
<b>Figure 3.7.</b> Histogram of lateral diameters of particles obtained from AFM data....	33
<b>Figure 3.8.</b> Cyclic voltammogram of catalyst I in 0.1 M $\text{HClO}_4$ at room temperature. Scan rate is 50 mV/s.....	34
<b>Figure 3.9.</b> Cyclic voltammogram of catalyst I in 0.1 M $\text{HClO}_4$ and MeOH at room temperature. Scan rate is 50 mV/s.....	35
<b>Figure 3.10.</b> Anodic part of the cyclic voltammogram of catalysts in 0.1 M $\text{HClO}_4$ + 0.5 M $\text{CH}_3\text{OH}$ at room temperature. Scan rate is 50 mV/s.....	36
<b>Figure 3.11.</b> Anodic part of the cyclic voltammogram of catalysts in 0.1 M $\text{HClO}_4$ + 0.5 M $\text{CH}_3\text{CH}_2\text{OH}$ at room temperature. Scan rate is 50 mV/s. ....	36
<b>Figure 3.12.</b> Anodic part of the cyclic voltammogram of catalysts in 0.1 M $\text{HClO}_4$ + 0.5 M 2-propanol at room temperature. Scan rate is 50 mV/s. ....	37
<b>Figure 3.13.</b> Chronoamperometric curves of methanol oxidation on catalyst I (a), II (b), III (c) and IV (d) at 0.6 V (vs. SCE) in 0.1 M $\text{HClO}_4$ + 0.5 M $\text{CH}_3\text{OH}$ .....	41

## CHAPTER 1

### INTRODUCTION

#### 1.1. THE CONCEPT OF FUEL CELL

World's growing population and improvements in technology cause increase in consumption of energy. As a matter of fact, world's energy need is predicted to grow 2.7 percent per year between 2003 and 2030<sup>1</sup>. On the other hand, in the near future, energy supplies, which are already diminishing, will not fulfill the whole demand. In fact, it is estimated that the world petroleum reserves will be dry in 40 years due to this consumption growth<sup>2</sup>. Also, most of the petroleum supplies are placed in countries which constantly undergo political instabilities and this causes volatile prices. Besides the economical drawbacks, the world suffers from the pollution caused by fossil fuels in nature. After burning of fossil fuels, considerable amount of sulfur dioxide (SO<sub>2</sub>), nitrogen oxides (NO<sub>x</sub>) and carbon dioxide (CO<sub>2</sub>) are released to the air. SO<sub>2</sub> and NO<sub>x</sub> cause not only the air pollution but also the acid rains<sup>3</sup>. Therefore, scientists have been trying to replace fossil fuels with renewable and environmentally friendly fuel sources and fuel processing systems. The main alternative and environmentally friendly energy production systems are solar energy systems, fuel cells, geothermal resources and wind power generation.

Nowadays, fuel cell, which is an electrochemical device that converts the chemical energy of fuel into electrical energy, is getting considerable interest among other alternative renewable energy systems due their advantages that they provide. These advantages can be summarized as:

- Fuel cells can be very small in size that can be used as battery of a cellular phone.

- The operation mechanism of fuel cell is quite simple. Basically, two different supplies are required for the fuel cell to operate namely, fuel and oxidant. Fuel is oxidized in the anode part and oxygen is reduced in the cathode part in the presence of an electrolyte. Electrolyte provides flow of current by transport of ions<sup>4</sup>.
- Fuel cells are environmentally friendly. In terms of electricity production, besides fuel cells, internal combustion engines are still in use. However, the use of fuel cells provides environmental advantages over burning fuel processes because in fuel cell reactions pollutants such as NO<sub>x</sub> and SO<sub>2</sub> are not produced while in conventional power generation methods they are. Moreover, in fuel cells, hydrogen, hydrocarbons, and basic alcohols are the main options that are employed as fuel. The origin of these fuels is nature itself and the products that are created from these processes do not have the harmful effect on nature the way fossil fuels do.
- The fuel cell economy makes the world energy economy independent of having a fuel source problem and unstable fuel pricing. In today's world, fossil fuels like gasoline and natural gas are the main sources that are used in energy production. Fuel cell technology provides an opportunity to replace fossil fuels.
- The other advantage of fuel cells is that fuel cells do not require recharging like batteries and other types of electrical storage devices. Fuel cells produce electricity, as long as fuel and oxidant are provided, by utilizing the potential energy in the fuel.
- Being silent is one of the best qualities of fuel cell technology and this advantage enables them to be used for indoor and residential purposes. Also, they are more favorable for car engines because of their quiet and steady operating mode.

Due to these advantages, fuel cells have wide range of applications and some of them are;

- Portable devices such as cell phones, laptops and small electronic devices.
- As a power source for car and bus engines.
- Generators for residential purposes.

On the other hand, for further applications, fuel cell technology is still waiting to be developed. Fuel cells are not cost effective because the materials that are used in this technology are not cheap and the construction costs of the cell are still high. In addition to those, there are some obstacles for fuel cell technology to be applied in transportation. Some of them are refueling and the starting time of fuel cell vehicles which are still longer and the driving range is shorter than that of a “normal” car<sup>5</sup>.

## **1.2.THE BRIEF STORY OF FUEL CELL TECHNOLOGY**

The idea of generating inexhaustible electrical energy was discovered through an interesting experiment involving connecting metal with the muscles of a frog. This discovery opened the door for different fields in electrochemical power sources. After Italian physiologist Luigi Galvani demonstrated this with his experiment in 1791, Italian physicist Alessandro Volta invented the first example of an electrochemical cell called “Volta pile” in 1800. With this invention, extraordinarily significant developments in the science of both electricity and electrochemistry were recorded because a continuous electrical current was no longer a dream.

In 1802 the production of hydrogen and oxygen, by electrolyzing water, was achieved by William Nicholson and Sir Anthony Carlisle. Following that, Sir William Robert Grove conducted a series of experiments on water electrolysis. He constructed a cell represented in Fig.1.1 by dipping two platinum electrodes into water acidified with sulfuric acid. By applying a current through water, hydrogen and oxygen were produced and electrolysis was achieved. He thought that there might be a possibility for the reverse reaction to produce energy. He also observed that despite disconnecting the current, the electrodes were still polarized which meant that a certain potential difference was preserved between electrodes. This day can be

accepted as birthday of the fuel cell. He also stated that such cells could be improved by increasing contact area between the gases, adsorbent and electrolyte<sup>6</sup>.

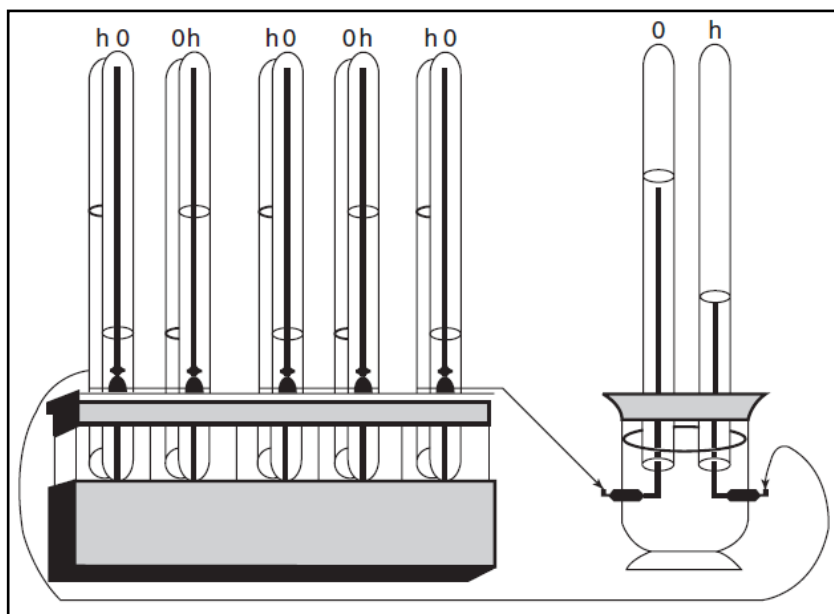


**Figure 1. 1.** Grove's gas battery (1839).

In 1889, Ludwig Mond and Carl Langer carried out experiments producing electricity from a hydrogen-oxygen cell. They tried to expand the surface of the platinum catalyst but the cost, reproducibility and performance problems made their study practically non-applicable. After them, in 1894 German physical chemist Wilhelm Ostwald came up with an idea which stated that generating electrical current with electrochemical methods would not be blocked by thermodynamic limitations.

In the first half of the 20th century, Emil Baur and his co-workers put great effort towards the electrochemical oxidation of coal and coal gasification studies. They constructed a cell that consisted of nickel, iron or platinum electrodes at the anode part, molten silver at the cathode part and they used molten carbonates like sodium or potassium carbonates as electrolytes. In addition to Baur's work, Armenian scientist Oganeg Davtyan worked on an electrolyte with higher conductivity and more

mechanical and chemical stability by using Urals' monazite sand, tungsten trioxide, calcium oxide, quartz and clay. The cell constructed by him operated much longer than former cells.

In 1932, Francis Thomas Bacon made improvements on alkaline fuel cells. He modified the Mond-Langer battery by changing the corrosive electrolyte acid solutions with alkaline electrolytes. To improve the resistance against corrosion, he treated nickel powdered electrodes with hot lithium hydroxide solutions. This cell was named as the Bacon cell and patented in 1959. Following Bacon, Grubb and Niedrach accomplished the electrochemical oxidation of hydrocarbons, like methane and ethane, by using the same platinum catalyst at temperatures below 150 °C. This study also pointed out the possibility of direct conversion of chemical energy of natural fuel to electrical energy.

In the second half of 20th century, fuel cells started to be commercialized by companies. The interest towards all types of fuel cell technology was growing sharply. Pratt & Whitney, which is an aircraft and engine manufacturer, got a license to use Bacon's patent and improved the design and implemented it with new technology. The company used this lower weight battery in the Apollo program for space flights to the Moon.

Grubb, Niedrach and their co-workers with the support of General Electric invented a new type of fuel cell using a solid membrane as an electrolyte (Proton Exchange Membrane Fuel Cell: "PEMFC"). This newly designed fuel cell was implemented in the Gemini project for space flights. During this time, NASA showed great interest in PEMFCs.

Applicable models of molten carbonate fuel cell (MCFC) investigations had been done since 1960 in universities. It was found that fuel itself can undergo an internal conversion to hydrogen and the advantage was that reforming was no longer necessary in a MCFC. With these improvements, companies from all around the world showed great interest towards MCFCs. During these years, there were other improvements that had been achieved beside MCFCs. In light of Davtyan's work,

high temperature solid oxide fuel cells were examined in lots of laboratories and improved, also; analogous and operating models were done and built. Likewise, the phosphoric acid fuel cell (PAFC) was introduced to market and generated great interest. With this technology, numerous power plants for hotels, hospitals and even entire cities were built in the United States, Japan and some other countries. Furthermore, direct liquid fuel cells were invented around 1960's and studied by many groups. Acids were used as electrolytes and hydrazine and methanol as fuel<sup>1</sup>.

After the 1980's, except for power plants, with the advancement of technology, scientists started to think that fuel cells could be used for different purposes by reducing their size. Till then it was believed that hydrogen was a good source for electro-oxidation, the contact surface of the catalyst was important and burning fuels had harmful effects on nature. However, there was an obstacle to overcome; the storage of hydrogen in its gaseous state was very hard. There was a search for another source which was more convenient, easy to handle, store and transport. In the end, scientist figured out that methanol was a more suitable source than gaseous hydrogen.

There are two different possible ways for the use of methanol in direct methanol fuel cells (DMFCs); the conversion of methanol to technical hydrogen by oxidizing or catalytic conversion to be used in PEMFCs, and the second way is the direct oxidation of methanol at the electrode of anode compartment. Since DMFC can be relatively small in size they are now attracting the interest of car manufacturers for the construction of electric cars and have become popular in the use of portable device's power source like laptop and cell phone batteries.

### **1.3.TYPES OF FUEL CELLS**

Fuel cells can be divided into three categories according to their operating temperature; low temperature, medium temperature and high temperature fuel cells. Polymer electrolyte membrane fuel cells (PEMFCs) are an example of low temperature fuel cells. Alkaline fuel cells (AFCs) and phosphoric acid fuel cells (PAFCs) are the subcategories of medium temperature fuel cells. Lastly, solid oxide

fuel cells (SOFCs) and molten carbonate fuel cells (MCFCs) are examples of high temperature fuel cells. In Table 1.1, major types of fuel cells are given and their main features are mentioned. By looking at their characteristics, such as operating temperatures, the amount of power that they generate or the type of fuel that they are using, it is easy to guess their application areas<sup>7</sup>.

**Table 1. 1.** Types of fuel cells, their main properties and some applications<sup>8</sup>.

Fuel Cell Type	Common Electrolyte	Operating Temperature	System Output	Electrical Efficiency	Combined Heat and Power (CHP) Efficiency	Applications	Advantages
<b>Polymer Electrolyte Membrane (PEM)*</b>	Solid organic polymer poly-perfluorosulfonic acid	50 - 100°C 122 - 212°F	<1kW – 250kW	53-58% (transportation) 25-35% (stationary)	70-90% (low-grade waste heat)	-Backup power -Portable power -Small distributed generation -Transportation -Specialty vehicles	-Solid electrolyte reduces corrosion & electrolyte management problems - Low temperature - Quick start-up
<b>Alkaline (AFC)</b>	Aqueous solution of potassium hydroxide soaked in a matrix	90 - 100°C 194 - 212°F	10kW – 100kW	60%	>80% (low-grade waste heat)	- Military - Space	- Cathode reaction faster in alkaline electrolyte, leads to higher performance -Can use a variety of catalysts
<b>Phosphoric Acid (PAFC)</b>	Liquid phosphoric acid soaked in a matrix	150 - 200°C 302 - 392°F	50kW – 1MW (250kW module typical)	>40%	>85%	-Distributed generation	- Higher overall efficiency with CHP - Increased tolerance to impurities in hydrogen
<b>Molten Carbonate (MCFC)</b>	Liquid solution of lithium, sodium, and/or potassium carbonates, soaked in a matrix	600 - 700°C 1112 - 1292°F	<1kW – 1MW (250kW module typical)	45-47%	>80%	- Electric utility - Large distributed generation	- High efficiency - Fuel flexibility - Can use a variety of catalysts - Suitable for CHP
<b>Solid Oxide (SOFC)</b>	Yttria stabilized zirconia	600 - 1000°C 1202 - 1832°F	<1kW – 3MW	35-43%	<90%	- Auxiliary power - Electric utility - Large distributed generation	- High efficiency - Fuel flexibility - Can use a variety of catalysts - Solid electrolyte reduces electrolyte management problems - Suitable for CHP - Hybrid/GT cycle

## **1.4. DIRECT LIQUID FUEL CELLS**

Different types of fuels and electrolytes can be employed in polymer electrolyte membrane fuel cells. Methanol is the first fuel used in the background of Direct Liquid Fuel Cells (DLFCs). After that, scientists have tried to replace the source to investigate the consequences. Nowadays, methanol, ethanol, formic acid, borohydrides and hydrazine are the main fuel types of direct liquid fuel cells (DLFCs), however; longer chain alcohols like propanol and butanol with potential higher energy content per unit mass are getting attractive.

### **1.4.1. DIRECT METHANOL FUEL CELL**

Among others direct methanol fuel cells have gotten considerable notice because of their benefits. These benefits can be classified as:

- In DMFC, methanol is employed as fuel. Methanol is highly convenient. Because it has a higher energy density than gaseous hydrogen. Also, it is liquid at room temperature so it is easier to handle and store. In addition to those, methanol can be sold just like gasoline in petroleum stations. Although, it has lower specific energy content than gasoline; due to its high energy conversion efficiency it is still taken into consideration by car manufacturers<sup>9</sup>.
- DMFCs are easily applicable for portable devices since they are relatively small in size. DMFCs have already begun to be utilized for cell phones, laptops and other electronic devices.
- The operating temperature of a DMFC is another enviable advantage because it is obvious that not only other types of fuel cells but PEMFCs also operate at higher temperatures<sup>5</sup>.

There are two compartments in a DMFC; anode compartment where the fuel is oxidized and cathode compartment where the oxygen is reduced by hydrogen.

Mostly acidic electrolytes are used because they provide removal of carbon dioxide without undergoing any reaction which occurs in alkaline electrolytes. As it is shown in Fig.1.2, the oxidation reaction of aqueous methanol that takes place at the anode side, carbon dioxide, protons and electrons come off. At the cathode side, water evolves out of the reaction between protons and oxygen. The electrochemical values of current-generating reactions are as follows<sup>6</sup>;

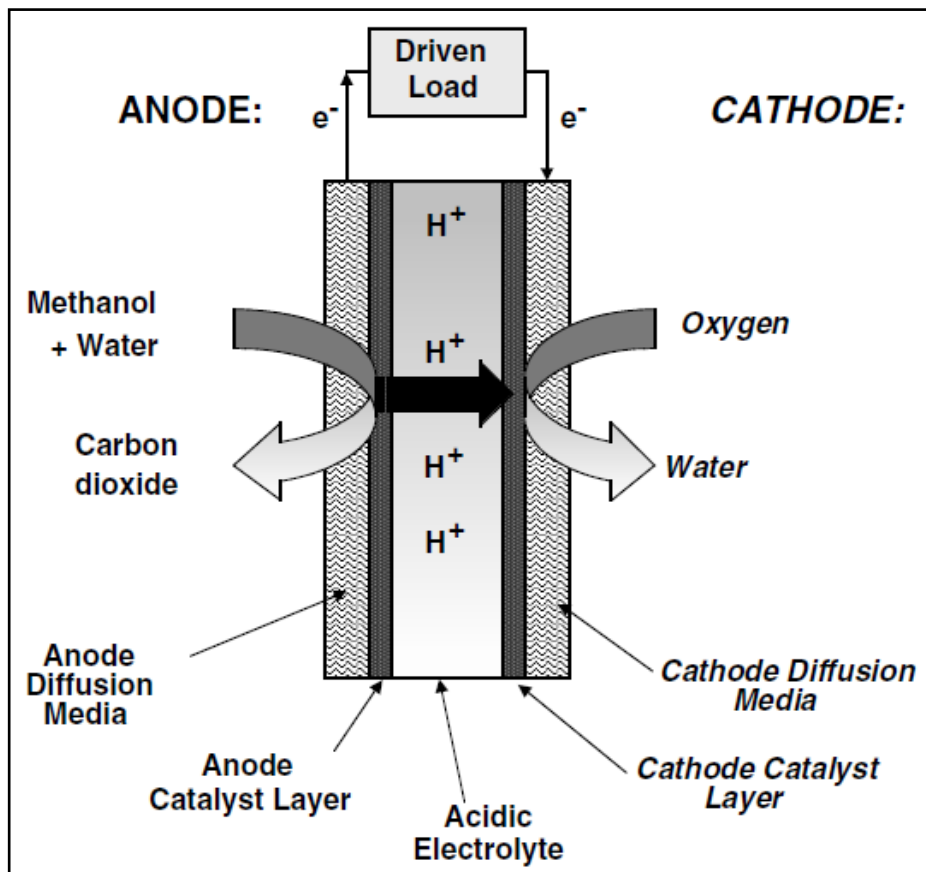
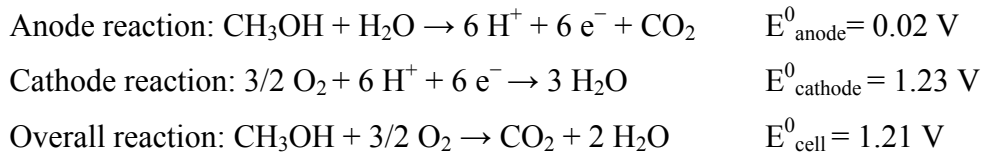
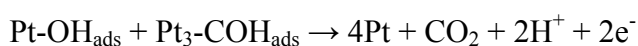
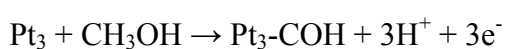


**Figure 1. 2.** Schematic representation of DMFC with solid acid electrolyte<sup>4</sup>.

Since the invention of DMFCs, many scientists have worked on the reaction mechanism of electro-oxidation of methanol on the surface of the catalyst to explain how methanol is adsorbed on the surface, the reactions that methanol undergoes and the side products of these reactions. In 1988 Parsons and Vandernoot summarized the proposed mechanism into two steps for methanol electro-oxidation. In the first step, methanol is electrochemically adsorbed onto the surface of the catalyst and carbon-containing intermediates, such as  $\text{Pt}_3\text{COH}$ , are formed. These carbon-containing intermediates generate carbon dioxide by addition of oxygen (from water or hydroxide) in the second step. These reactions can be shown<sup>4</sup>:



When these reactions occur, there may be generation of side products, such as formaldehyde and formic acid. It is also possible to produce carbon monoxide adsorbed onto platinum surface, which is called as poisoning, Figure 1.3. This prevents the further electro-sorption of methanol and blocks the methanol oxidation reaction.

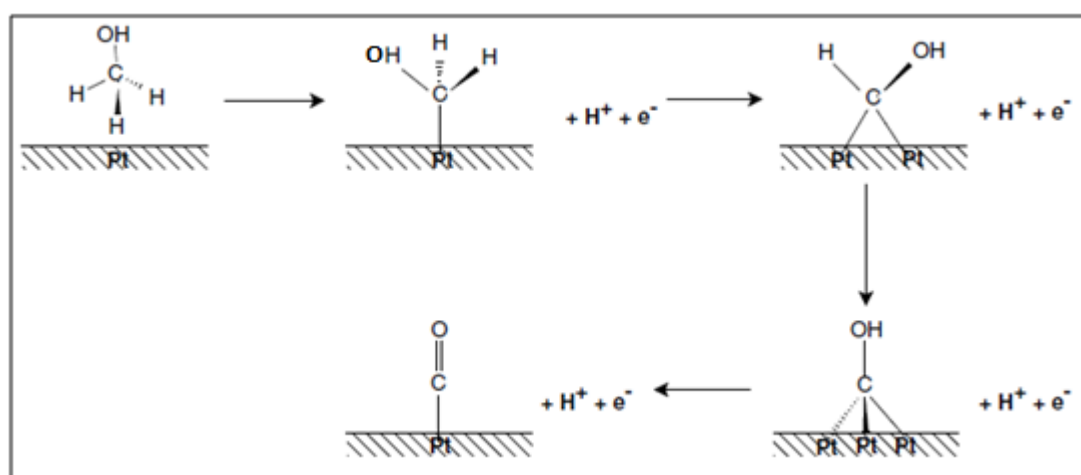


**Figure 1.3.** Formation of poisoning ( $\text{CO}_{\text{ads}}$ ) on the surface of the platinum.<sup>4</sup>

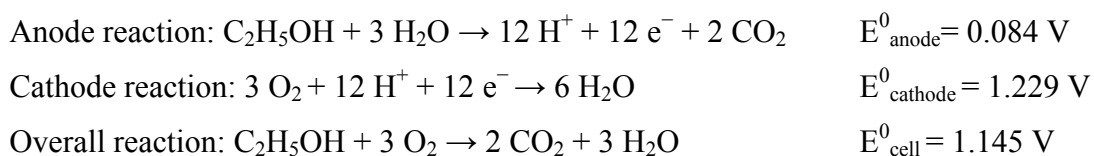
Despite the improvements on DMFCs, they still do not have a wide range of practical applications and are not fully commercialized because of some drawbacks. These are a) rate of reaction; the anodic reaction of methanol is very slow and there are still many ongoing researches to improve the activity of anode catalysts, b) life time of DMFC; the testing for the lifetime estimation of DMFCs is not reliable yet and this hinders the applications of the DMFCs in real life, c) price of DMFC; the noble metals like platinum, ruthenium or palladium are very expensive and this causes the high cost of catalyst production for DMFCs.

#### 1.4.2. DIRECT ETHANOL FUEL CELL

After the considerable success in the oxidation of methanol, scientists started looking for another fuel having more electrochemical potential. The answer was obviously sought in the relatives of methanol and the first choice was ethanol.

Ethanol, which is also known as a green fuel, is a shining alternative because it has higher energy density than methanol. The most important feature of ethanol is its renewability. Ethanol, which is derived from plant respiration of carbon dioxide, can be obtained in great quantities from biomass after fermentation of such renewable sources like sugar cane. Carbon dioxide is one of the products in the oxidation of ethanol in fuel cells and is used by plants in photosynthesis.

The electrochemical values of current-generating reactions in DEFC theoretically are as follows<sup>6</sup>;



As in the electro-oxidation of methanol, resultant products show variations for ethanol case. Carbon dioxide and water are not the only products released. Also the side product generation is occurred. There are different points of view about this issue. First research was held by Arico et al. with chromatographic methods and they found that the main product is carbon dioxide about 98%. However, Wang et al.

analyzed the yields with mass spectroscopy and stated that acetaldehyde accompanies carbon dioxide as a major product with the percentage of 60 to 80. As a last work on yields handled by Rousseau et al. with high performance liquid chromatography in 2006 and they claimed that there are three products belongs to electro-oxidation of ethanol and they are aldehyde, acetic acid and carbon dioxide. The proposed mechanisms for formation of these products are as follow<sup>6</sup>;

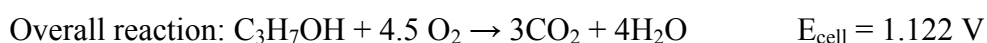
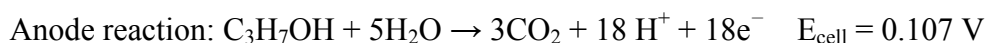


The formation of these side products can be attributed to the difficulty of rupture C-C bond in ethanol because the cleavage reaction and the formation of carbon dioxide may not take place under 200 °C. Another disadvantage of ethanol is the significantly slower electro-oxidation of ethanol relative to methanol. Although these drawbacks, DEFCs are still eye catching technology due to the fact that ethanol is generated by nature itself.

### 1.4.3. DIRECT 2-PROPANOL FUEL CELL

During the last decade, high energy density of longer chain alcohols succeeded to catch the attention of scientists dealing with fuel cell. 1-propanol and 2-propanol are the main candidates. Due to its molecular shape, 2-propanol (secondary alcohol) gets great interest because of the lower tendency exhibited by secondary alcohols to adhere to the platinum surface<sup>10</sup>. Also, 2-propanol is less toxic than methanol and it provides three times more protons and electrons for the cathode reaction in direct 2-propanol fuel cells (D2PFCs)<sup>11</sup>.

The electrochemical values of current-generating reactions in D2PFCs theoretically are as follows<sup>12</sup>;



The pathway of electro-oxidation reaction of 2-propanol is certainly more complex than smaller chain alcohols like methanol and ethanol. There are two different approaches for determining the products yielded in electro-oxidation of 2-propanol. First study stated that two products liberate in the reaction and they are acetone and carbon dioxide with approximately same percentages<sup>13</sup>. In second work, Wang et al. studied with multipurpose electrochemical mass spectrometer in a cell with the Pt-Ru and Pt catalysts towards electro-oxidation of 2-propanol and they concluded that most of the yield is 2-propanone and the minor product is carbon dioxide (wang,wasmus,savinell). The proposed reaction is as follow<sup>11</sup>,



### **1.5.THE CONCEPT OF NANOPARTICLE**

The particle with size range between 1 to 100 nm can be named as nanoparticle or submicron particle. As solid particles are brought to nano-scale, the tendency in their behavior is affected by the atoms or molecules of themselves which results in different properties of the same material compared to bulk. It can be attributed to the change of the bonding state of the atoms or the molecules consisting in the particles. The atoms or molecules which are located on the surface play a great role because the reaction occurs on these atoms or molecules<sup>14</sup>.

It is a known fact in the presence of a catalyst the activation energy of the reaction would decrease by changing the pathway and it causes acceleration at the reaction rate. As mentioned above, the contact area is very important to improve the properties of the particles and with this aspect the activity of the catalyst can be improved by increasing the surface of it. However, with the superior activity, nanoparticles have tendency to merge into another until one large particle remains which can be described as agglomeration. Therefore, to prevent aggregation to bulk, there are main methods for stabilization of metal colloidal particles<sup>15</sup>.

- Electrostatic stabilization
- Steric stabilization

- Electrosteric stabilization
- Stabilization by a ligand or a solvent

In electrostatic stabilization, finely distributed particles can be stabilized by utilizing the ionic species such as halides, carboxylates or polyoxoanions. As it is represented in Fig. 1.4., there is a generation of double layer resulting in confined particles by the ionic compounds owing to Coulombic repulsion between nanoparticles.

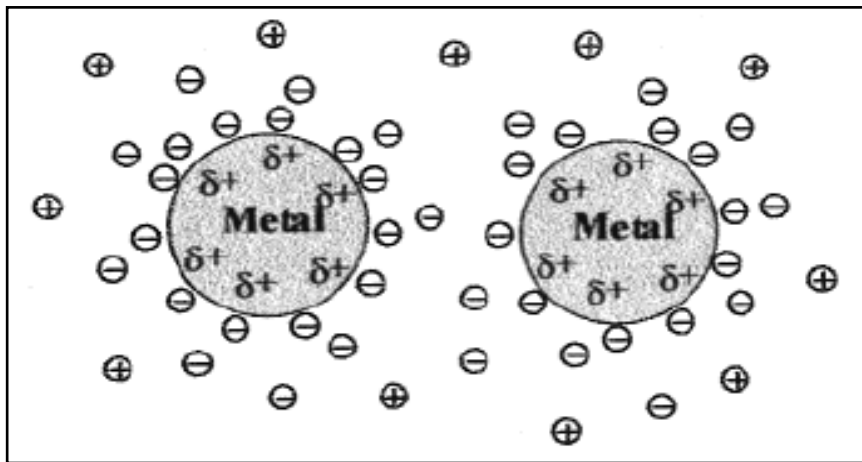


**Figure 1.4.** Schematic representation of electrostatic stabilization<sup>15</sup>.

As a second way in the steric stabilization, polymers or oligomers are used as stabilizing agents to prevent agglomeration. The adsorption of these species (surfactant) creates a protective layer which keeps the nano-sized particles away from each other (Fig. 1.5.). In addition to that, the length and nature of the surfactant has an influence on the thickness of the layer and thus, has an effect on nanoparticles.

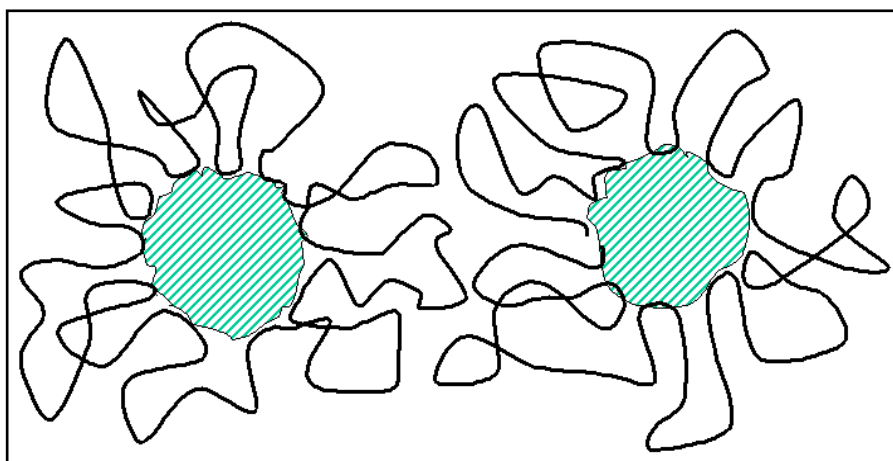


**Figure 1.5.** Schematic representation of steric stabilization<sup>16</sup>.

As it can be understood from the name, the electrosteric stabilization is a combination of electrostatic stabilization and steric stabilization. In this type of stabilization, more complex surfactants, a polar head to surround the particle and lypophilic tail provides steric repulsion in solvent, are used to maintain the stability of metal particles (Fig. 1.6.).

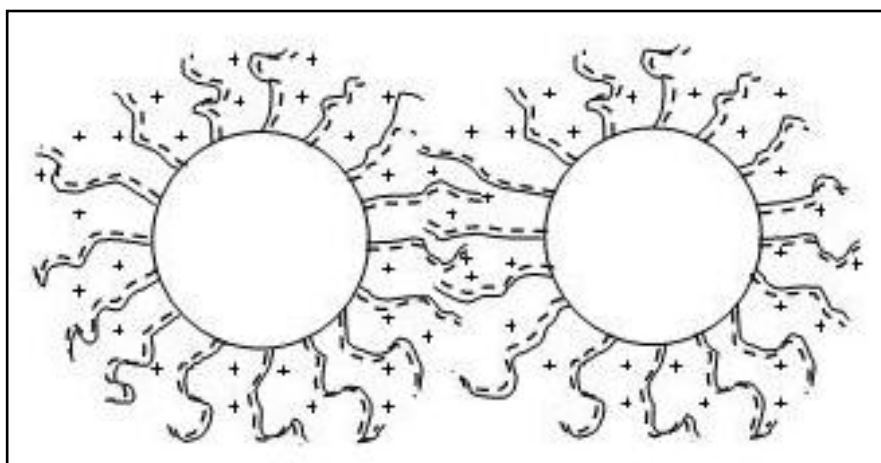


**Figure 1.6.** Schematic representation of electrosteric stabilization<sup>17</sup>.

Lastly, ligand stabilization is used for stabilizing the transition metal colloids by protecting them from aggregation. Dissolved metal nanoparticles coordinate with ligands such as phosphines, thiols, amines or carbon monoxide. Also, stabilization of the metal nanoparticles can be done without using any stabilizing agents just by dissolving of the metal in solvent such as tetrahydrofuran and thioethers<sup>13</sup> (Fig. 1.7.).

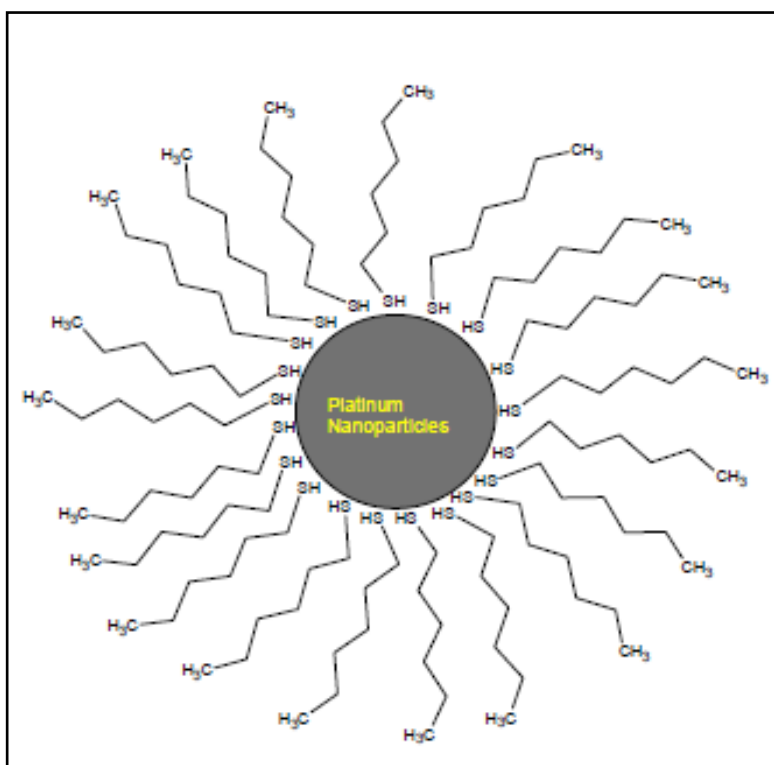


**Figure 1.7.** Schematic representation of ligand stabilization<sup>18</sup>.

## 1.6. THE AIM OF THE WORK

As mentioned before, the reaction rate of electrochemical oxidation of alcohols at the anode compartment is very low. Until today, most of the studies show that platinum catalysts show a reasonable reaction rate and longer stability<sup>4</sup>. On the other hand, the amount of Pt that is used in the system is also important. Because the increase in the amount of Pt used in the fuel cell causes an increase in the cost of fuel cell. To

overcome this problem Pt was begun to be used as nanoparticle form because while the surface area of the Pt is getting increase, the number of Pt atoms, which involve in the reaction, increase. In order to get Pt nanoparticles, ligand stabilization method, which is one of the methods for stabilization of metal nanoparticle, was used. These ligands are used to keep the nano-sized metal particles away from agglomeration.

In this thesis, platinum nanoparticles were synthesized by using surfactants with different length; 1-octanethiol ( $C_8H_{18}S$ ), 1-decanethiol ( $C_{10}H_{22}S$ ), 1-dodecanethiol ( $C_{12}H_{26}S$ ) and 1-hexadecanethiol ( $C_{16}H_{34}S$ ) to observe the effect of chain length of the surfactant on the particle size of metal (Pt), to be used at anode electrode where the electro-oxidation of alcohols takes place in acid media. In the characterization, percent platinum content of nanoparticles is determined with inductively coupled plasma-mass spectroscopy (ICP-MS), particle size and structure were characterized by transmission electron microscopy (TEM) and X-ray diffraction (XRD), the chemical compositions on the selected area and the oxidation states of the prepared Pt nanoparticles were studied by X-ray photoelectron spectroscopy (XPS) and electrochemical properties of the prepared catalyst, efficiency and activity, were determined with cyclic voltammetry.

## CHAPTER 2

### EXPERIMENTAL

#### 2.1. SYNTHESIS OF CATALYSTS

##### 2.1.1. SYNTHESIS OF THE CATALYST I

0.24 mmol (0.0808 g) of  $\text{PtCl}_4$  (99%, Alfa) was dissolved by stirring vigorously in 25 ml of anhydrous tetrahydrofuran (THF, 99.5%, Merck) for an hour. 0.24 mmol (42 $\mu\text{L}$ ) of 1-octanethiol was added to the solution and was stirred for 2.5 hours. Then, lithium triethylborohydride (superhydride, 1.0 M dissolved in THF, Aldrich) was added dropwise to reduce these nanoparticles until the color of the solution completely turns yellowish to black which is the sign of generation of reduced nano-sized Pt particles. Also, hydrogen gas liberation was clearly observed during the addition of superhydride<sup>19</sup>. After the synthesis of Pt nanoparticles, the excess thiol surfactants were removed by the following process. The precipitate was washed in dry ethanol (99.9%, Merck) in ultrasonic bath repeatedly and was centrifugated to precipitate the nanoparticles. This procedure followed until a clear solution of nanoparticle was observed. Finally, the clear solution was evaporated under vacuum at room temperature.

##### 2.1.2. SYNTHESIS OF CATALYST II, III, IV

The same amounts of  $\text{PtCl}_4$  (99%, Alfa) were used in the synthesis of catalysts II, III, and IV by following the same procedure explained in section 2.1.1. 1-decanethiol, 1-dodecanethiol and 1-hexadecanethiol were used as surfactants for catalyst II, III, IV respectively, Table 2.1.

**Table 2.1.** Platinum complexes and surfactant used for all the prepared catalysts.

Catalysts	Platinum complex	Surfactant
Catalyst I	PtCl <sub>4</sub>	1-octanethiol
Catalyst II	PtCl <sub>4</sub>	1-decanethiol
Catalyst III	PtCl <sub>4</sub>	1-dodecanethiol
Catalyst IV	PtCl <sub>4</sub>	1-hexadecanethiol

## **2.2. PREPARATION OF CARBON SUPPORTED PLATINUM CATALYST**

In order to get uniformly distributed Pt nanoparticles on carbon support, the prepared catalyst and the supporting material carbon XC-72 were mixed in a 1:10 ratio and stirred for three days<sup>20</sup>.

## **2.3. PREPARATION OF ELECTRODE SOLUTION AND APPLICATION ON ELECTRODE**

0.5 mL Nafion (5 wt %, Aldrich), 0.15 mL N,N-dimethyl formamide (99.5%, Merck) and 2.5 mL distilled water were added in 36.78 mg of carbon supported Pt catalyst. In order to get a homogenous solution, prepared mixture was sonicated in ultrasonic bath periodically.

50  $\mu$ L of electrode solution was poured on the surface of the glassy carbon with 0.7 cm diameter. To complete the preparation of the working electrode, drying process was applied by heating the electrode from 40 °C (20 min.) to 65 °C (20 min.) and finally to 100 °C (60 min.) gradually to get good adhesion.

## **2.4. DETERMINATION OF PLATINUM CONTENT IN THE CATALYSTS**

Leeman Lab inductively coupled plasma mass spectroscopy (ICP-mass) was utilized in the determination of Pt content of the prepared catalysts. (Central Lab., METU).

## **2.5. CHARACTERIZATION**

### **2.5.1. CYCLIC VOLTAMMETRY (CV) AND CHRONOAMPEROMETRY (CA)**

The cyclic voltammetry and chronoamperometry measurements were conducted with a microcomputer-controlled potentiostat/galvanostat, Solartron 1285, at room temperature (Department of Chemistry, METU). For all the measurements, electrochemical cell with three electrodes was utilized. These electrodes are the working electrode, which contains catalysts on its 0.7 cm glassy carbon surface, saturated calomel electrode (SCE) and reference electrode, which is made from glassy carbon. 0.1 M HClO<sub>4</sub> was used as electrolyte.

### **2.5.2. X-RAY DIFFRACTION (XRD)**

Particle size analysis were performed with Rigaku diffractometer with Ultima + theta-theta high resolution goniometer, the X-ray generator (Cu K $\alpha$  radiation,  $\lambda = 1.54056\text{\AA}$ ) with an operation conditions at 40 kV and 40 mA. The spectra were obtained at a scan rate of  $5^\circ \text{min}^{-1}$ , with steps of  $0.020^\circ$  in the  $2\theta$  scans. (Central Lab., METU).

### **2.5.3. TRANSMISSION ELECTRON MICROSCOPY (TEM)**

Transmission electron microscopy analysis was carried out with JEOL 200 kV TEM instrument to determine the size of platinum nanoparticles. Samples were prepared by using sonicated (10 min) CCl<sub>4</sub> suspension ( $\sim 0.5 \text{ mg/mL}$ ) of each catalyst. A drop of this suspension was deposited onto carbon covered 400-mesh copper grid and the solvent allowed evaporating at room temperature before TEM analysis. (Central Lab., METU).

#### **2.5.4. X-RAY PHOTOELECTRON SPECTROSCOPY (XPS)**

For X-ray photoelectron spectroscopy analysis, Specs spectrometer with an X-ray source, K $\alpha$  lines of Mg (1253.6 eV, 10 mA), was used (Central Lab., METU). All XPS peaks have been fitted by using Gaussian function and C 1s line at 284.6 eV was determined as a reference line.

#### **2.5.5. ATOMIC FORCE MICROSCOPY (AFM)**

The surface topographies of the prepared catalysts were imaged using a Digital Instruments Multi Mode AFM Nanoscope IV a (Veeco Ins., Santa Barbara, CA) (Department of Chemistry, METU). All measurements were performed using a 0.01-0.025 ohm-cm antimony doped silicon probes (Ultrasharp TESP, tip radius of about 2 nm and resonance frequencies of 328 - 379 kHz) having cantilever spring constants of 20–80 N/m, in the tapping mode at room temperature. AFM images were analyzed with a commercial software package, Nanoscope 6.13 (version 6.13.r1, Veeco). All prepared catalysts were suspended in a deionized water (~300 fold) using an ultrasonic bath and 2.5  $\mu$ L of the final solution was placed on the freshly cleaved mica disk (supporting material) and a solvent was allowed to evaporate at room temperature.

## CHAPTER 3

### RESULTS AND DISCUSSION

#### 3.1. X-RAY DIFFRACTION AND TRANSMISSION ELECTRON MICROSCOPY

The analysis of the crystalline structure and the particle size of metal (Pt) were performed by using X-ray diffraction (XRD) and transmission electron microscopy (TEM). As in Figure 3.1., broad peaks in the XRD patterns of all the catalysts at about  $2\theta = 39.60, 46.20, 67.40$  and  $81.50$  was assigned to Miller indices (111), (200), (220) and (311) for the planes of the face-centered cubic (fcc) crystal lattice of platinum<sup>21</sup>. The line broadening was the result of the small size of metal (Pt) particles. The additional peaks were also observed at  $2\theta = 21.35, 31.00, 31.65$  and  $59.00$ , Figure 3.1. In order to explain these peaks a blank is prepared by following the same method in the preparation of catalysts without using any  $\text{PtCl}_4$ . When the XRD spectrum of the blank sample is examined, these peaks can be attributed to the different Li compounds that could form during the reactions of surfactant and superhydride which could not be removed during cleaning process.

From full width half maximum of the (220) peaks in XRD, the average crystallite platinum particle size of all the catalysts was calculated using Scherrer equation<sup>22</sup>;

$$d (\text{\AA}) = \frac{k\lambda}{\beta \cos\theta}$$

where,

$k$ = a coefficient (0.9)

$\lambda$ = the wavelength of X-ray used (1.54056  $\text{\AA}$ )

$\beta$ = the full width half-maximum of respective diffraction peak (rad)

$\theta$ = the angle at the position of peak maximum (rad)

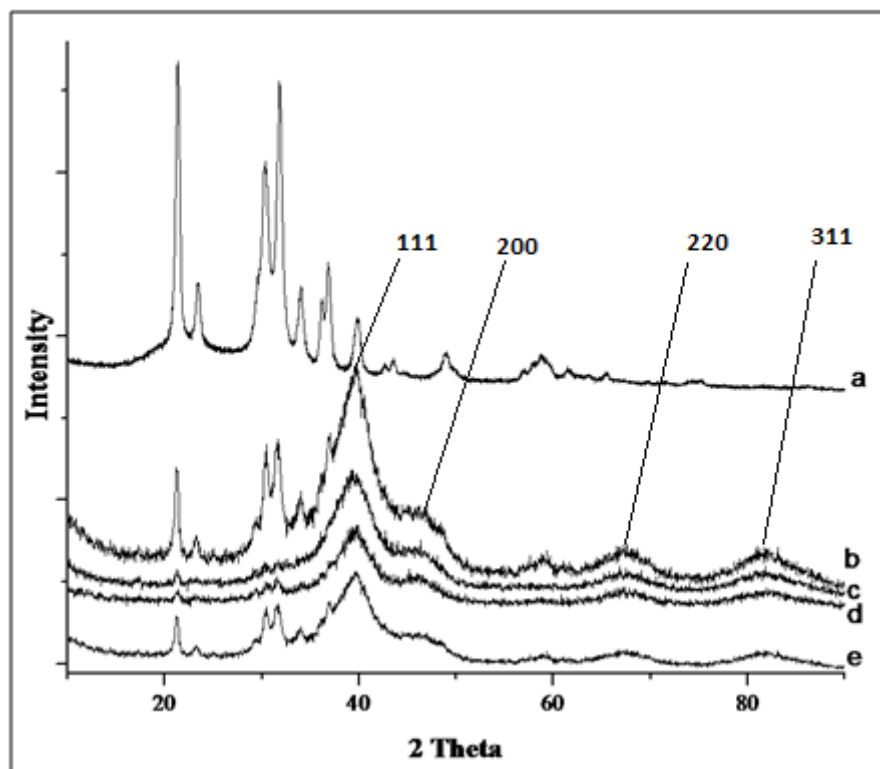


**Figure 3.1.** XRD of blank (a), catalyst I(c), II(d), III(e) and IV (b).

The average crystalline sizes of the catalyst I, II, III and IV were found to be about 1.92, 1.91, 1.87 and 1.48 nm, respectively. These results indicated that the size of crystalline platinum nanoparticles was dependent on the length of surfactants. It should be noted that as the chain length of surfactant increases, the size of platinum crystallites decreases, which were in good agreement with previous studies<sup>8</sup>. These studies state that the cavities which formed by the surfactant molecules, differs in size with respect to size of the surfactant molecules. The longer the chain is the smaller the cavity is<sup>23, 24, 25, 26, 27</sup>.

In order to solidify the results of diffraction measurements, transmission electron microscopy was used. The high resolution transmission electron micrograph and particle size histogram of the catalyst I are given in Figure 3.2., which is a representative of morphology of the other prepared catalysts as well. Uniform distribution of catalyst particles with a relatively narrow range on carbon support was observed. The average particle sizes were found to be,  $\sim 2.0 \pm 0.90$  nm,  $\sim 1.9 \pm 0.92$

nm,  $\sim 1.8 \pm 0.86$  nm and  $\sim 1.3 \pm 0.41$  nm for catalyst I, II, III and IV, respectively. These results were consistent with the X-ray diffraction results. In addition to these particles, a few large particles,  $\sim 50$ - $100$  nm diameters, were also observed in catalyst III and IV. These large sized particles are the result of the accumulation of the small individual particles, as shown in Figure 3.3. In addition to particle size analysis, the atomic lattice fringes have also been studied by high resolution transmission electron microscopy, shown in Figure 3.4. For instance, for catalyst I, Pt (1 1 1) and (2 0 0) planes was observed with spacing of 0.228 and 0.198 nm, respectively, which was very close to nominal Pt(1 1 1) and (2 0 0) spacing of 0.227 and 0.196 nm, respectively<sup>28, 29</sup>.

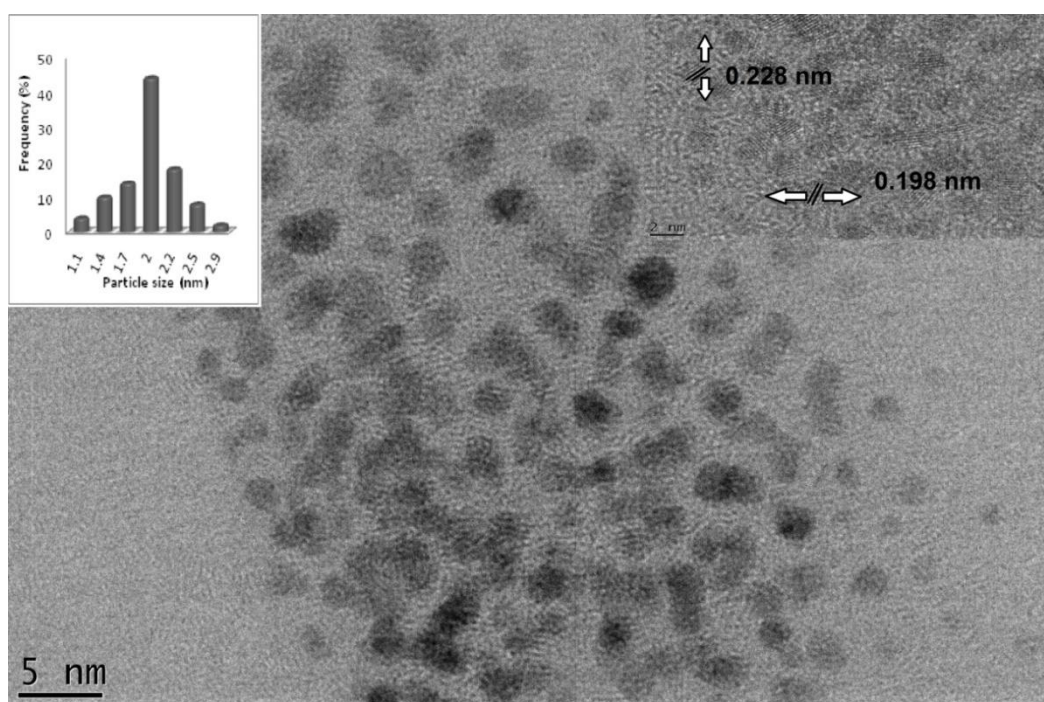


**Figure 3.2.** High resolution transmission electron micrograph and particle size histogram of a catalyst I.

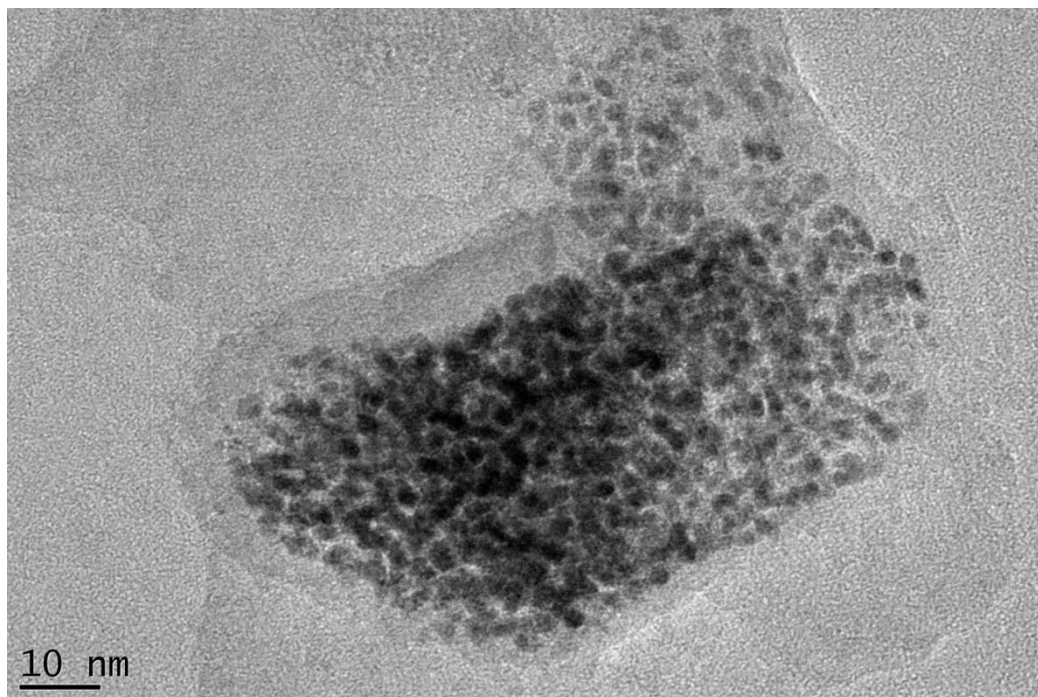


**Figure 3.3.** Transmission electron micrograph of catalyst III.

### **3.2. X-RAY PHOTOELECTRON SPECTROSCOPY:**

X-ray photoelectron spectroscopy (XPS) was used to investigate the oxidation state of platinum, oxygen and sulfur for the prepared catalysts. For this purpose, the Pt 4f, S 2p and O 1s regions of spectrum were analyzed. Gaussian-Lorentzian method was used for fitting of all XPS peaks and the background was subtracted by means of Shirley's method and all peaks were analyzed in terms of relative peak area and chemical shifts of Pt, S and O.

For all XPS spectrum, C1s peak (284.6 eV) was taken as a reference and the charging effects were corrected according to that value. As it was shown in Figure 3.4., the Pt 4f signal consists of two pairs of doublet which had almost equal half-widths with an intensity ratio of ca. 3:4 and the spin orbit splitting of 3.33 eV, and it was the most intense doublet ( $\sim 71.0$  and  $74.2$  eV) due to Pt (0)<sup>15</sup>. The other doublet of Pt was appeared in higher binding energies ( $\sim 74.3$  and  $77.8$  eV)<sup>30</sup> which can be attributed to the presence of Pt (IV) species such as PtO<sub>2</sub><sup>31</sup> and/or Pt(OH)<sub>4</sub><sup>32</sup> on the

surface. The XPS results of the all prepared catalysts for Pt 4f region were given in Table 3.1. Also, it can be concluded from Table 3.1. that the binding energy was shifted toward higher energy with decreasing particle size. This result can be ascribed to quantum confinement effect. According to this effect, the electronic features of the materials show variety while going from bulk to nano-size<sup>33</sup>. In the XPS spectrum of a bulk metal, conduction charge screens effectively the positive core hole. This causes a decrease in the final state energy which results in lowering in the measured binding energy. On the other hand in small clusters, instead of this metallic screening, it turns into a less efficient local process like polarization of neighboring atoms and that cause an increase in the binding energy<sup>34</sup>.

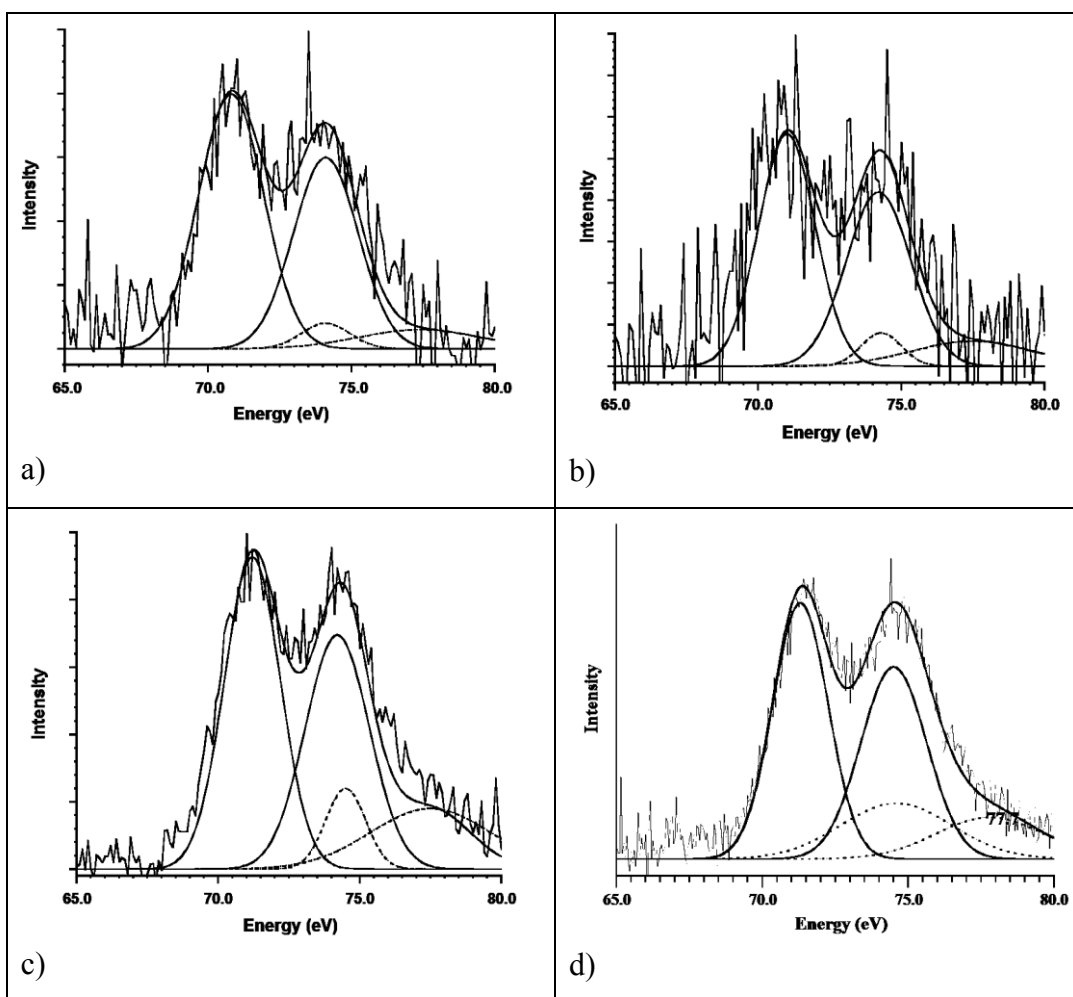


**Figure 3.4.** Pt 4f electron spectra of catalyst I (a), II (b), III (c) and IV (d).

**Table 3.1.** Pt 4f<sub>7/2</sub> core binding energies, eV, in the prepared catalysts. The number in the parentheses is the relative intensities of the species.

	Pt 4f <sub>7/2</sub>	Pt 4f <sub>7/2</sub>	
Catalysts	Pt(0)	Pt(IV)	Pt(0)/Pt(IV)
Catalysts I	70.8 (89.1)	74.1 (10.9)	8.17
Catalysts II	71.0 (84.9)	74.2 (15.1)	5.62
Catalysts III	71.2 (75.6)	74.1 (24.4)	3.10
Catalysts IV	71.3 (72.1)	74.5 (27.9)	2.58

A single O 1s peak appeared at 531.7 and 532.5 eV for catalyst III and IV, respectively and a doublet O 1s peaks was obtained at 531.5 eV (71.4 %), 533.2 eV (28.6 %) and 531.6 (79.3 %), 533.3 eV (20.7 %) for catalyst I and II, respectively by the help of Gaussian curve fitting analysis with a half width of about 1.6 eV for all catalysts, Table 3.2. It is believed that these peaks are due to adsorbed hydroxide<sup>35</sup> (at ~531.5 ± 0.5 eV) and adsorbed water<sup>36</sup> (at ~533.0 ± 1.0 eV) on the surface of the catalyst I and II as % 28.6 and % 20.7, respectively.

**Table 3.2.** O 1s core binding energies, eV, in the prepared catalysts. (The numbers in the parentheses are the relative intensities of the species).

	O 1s (eV)	O 1s (eV)
Catalysts	Adsorbed hydroxide	Adsorbed water
Catalysts I	531.5 (71.4)	533.2 (28.6)
Catalysts II	531.6 (79.3)	533.3 (20.7)
Catalysts III	531.7	-----
Catalysts IV	532.5	-----

The S 2p<sub>3/2</sub> region of XPS was also evaluated and, 2:1 peak area ratio and 1.2 eV splitting<sup>37</sup> were used as fitting parameters. The peak positions of two doublets were summarized in Table 3.3. for all prepared catalysts with binding energies of 162.0 – 162.3 eV. This shift is most probably due to a sulfur atom bounded to the platinum surface. Also, the reasons for the peaks with binding energies varying from 164.0eV to 164.6 eV were assigned to the unbounded thiol groups<sup>38</sup>.

**Table 3.3.** S 2p<sub>3/2</sub> core binding energies, eV, in the prepared catalysts. (The number in the parentheses is the relative intensities of the species).

	S 2p <sub>3/2</sub>	S 2p <sub>3/2</sub>	
Catalysts	bounded thiols (bt)	unbonded thiols (ut)	ratio (bt/ut)
Catalyst I	162.3 (60.2)	164.6 (39.8)	1.51
Catalyst II	162.1 (64.3)	164.5 (35.7)	1.80
Catalyst III	162.0 (68.2)	164.1 (31.8)	2.14
Catalyst IV	162.1 (71.3)	164.0 (28.7)	2.48

After all, the ratio of platinum to sulfur could be another parameter to estimate the catalytic activity of the catalysts. It indicates that the availability of the platinum surface for oxidation of alcohols. It was expected that the activity of the catalyst increases with the high Pt to sulfur ratio. Therefore, the Pt to sulfur ratio was calculated by using Pt 4f and S 2p areas in the XPS spectra and given in Table.3.4.

**Table 3.4.** Pt 4f and S 2p ratios determined by XPS.

Catalysts	Pt/S ratio
Catalyst I	6.8
Catalyst II	4.9
Catalyst III	3.5
Catalyst IV	2.1

### 3.3. ATOMIC FORCE MICROSCOPY

By means of atomic force microscopy (AFM), heights and lateral diameter distributions of Pt nanoparticles were examined at room temperature and the corresponding AFM images and results are given in Figures 3.5., 3.6., 3.7. and Table 3.5., respectively. The heights of the particles were found as 1.84, 1.81, 1.77 and 1.59 nm for catalysts I, II, III and IV, respectively. These results also exhibit similar trend with the XRD and TEM results. On the other hand, the AFM lateral diameters of the particles are much larger than the XRD and TEM owing to most probably tip contamination and/or the tip convolution. The accuracy of AFM lateral diameter determination can be improved by the deconvolution calculation. The tip deconvolution can be calculated by following formula<sup>39, 40</sup> using the mean half angle of the tip,  $\theta$  ( $17^\circ$ ), instead of apex radius due to larger lateral dimensions of the particles compared to the tip radius.

$$r_c = r[\cos\theta + (\cos^2\theta + (1 + \sin\theta)(-1 + (\tan\theta/\cos\theta) + \tan^2\theta))^{1/2}],$$

where  $r_c$  is the observed particle diameter and  $r$  is the real particle diameter. The observed particle diameters are 44.2, 46.8, 50.2 and 47.6 nm and the deconvoluted lateral radius of particles are 34.0, 36.0 and 38.6 and 36.6 nm for catalyst I, II, III and IV, respectively, (Table 3.5.). The large ratio of lateral radius to height may be attributed to aggregation of particles on the freshly cleaved smooth mica surface owing to tip indentation.

**Table 3.5.** Average crystallite platinum particles size determined by (a) X-ray line broadening, (b) transmission electron microscopy, (c) particle height, (d) observed lateral diameter and (e) deconvoluted lateral diameter determined by AFM.

Catalysts	a (nm)	b (nm)	c (nm)	d (nm)	e (nm)	e/c
Catalysts I	~1.92	~2.0 ±	~1.84 ±	~44.2	~34.0	18.5
Catalysts II	~1.91	~1.9 ±	~1.81 ±	~46.8	~36.0	20.0
Catalysts III	~1.87	~1.8 ±	~1.77 ±	~50.2	~38.6	21.8
Catalysts IV	~1.48	~1.6 ±	~1.59 ±	~47.6	~36.6	23.0

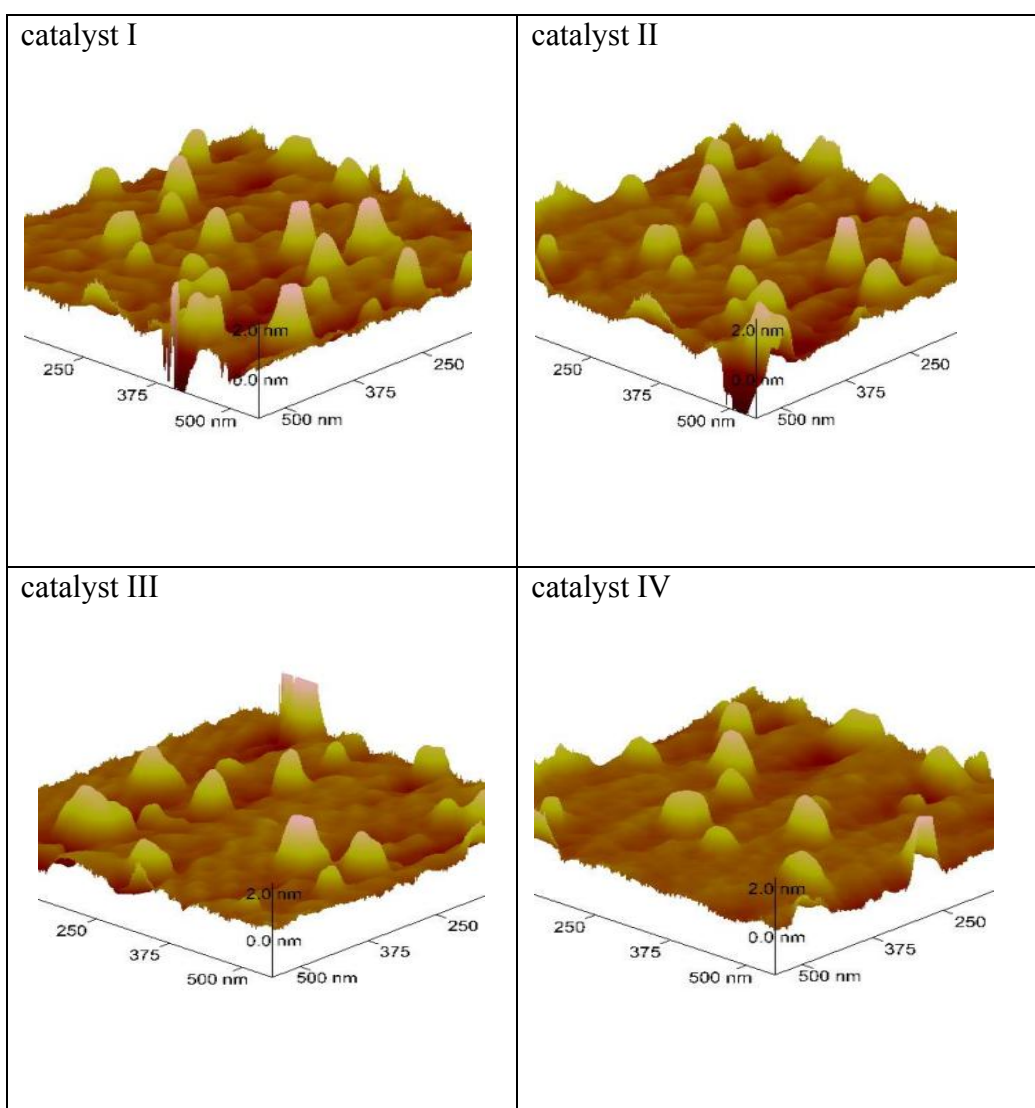


**Figure 3.5.** AFM images of the catalysts.

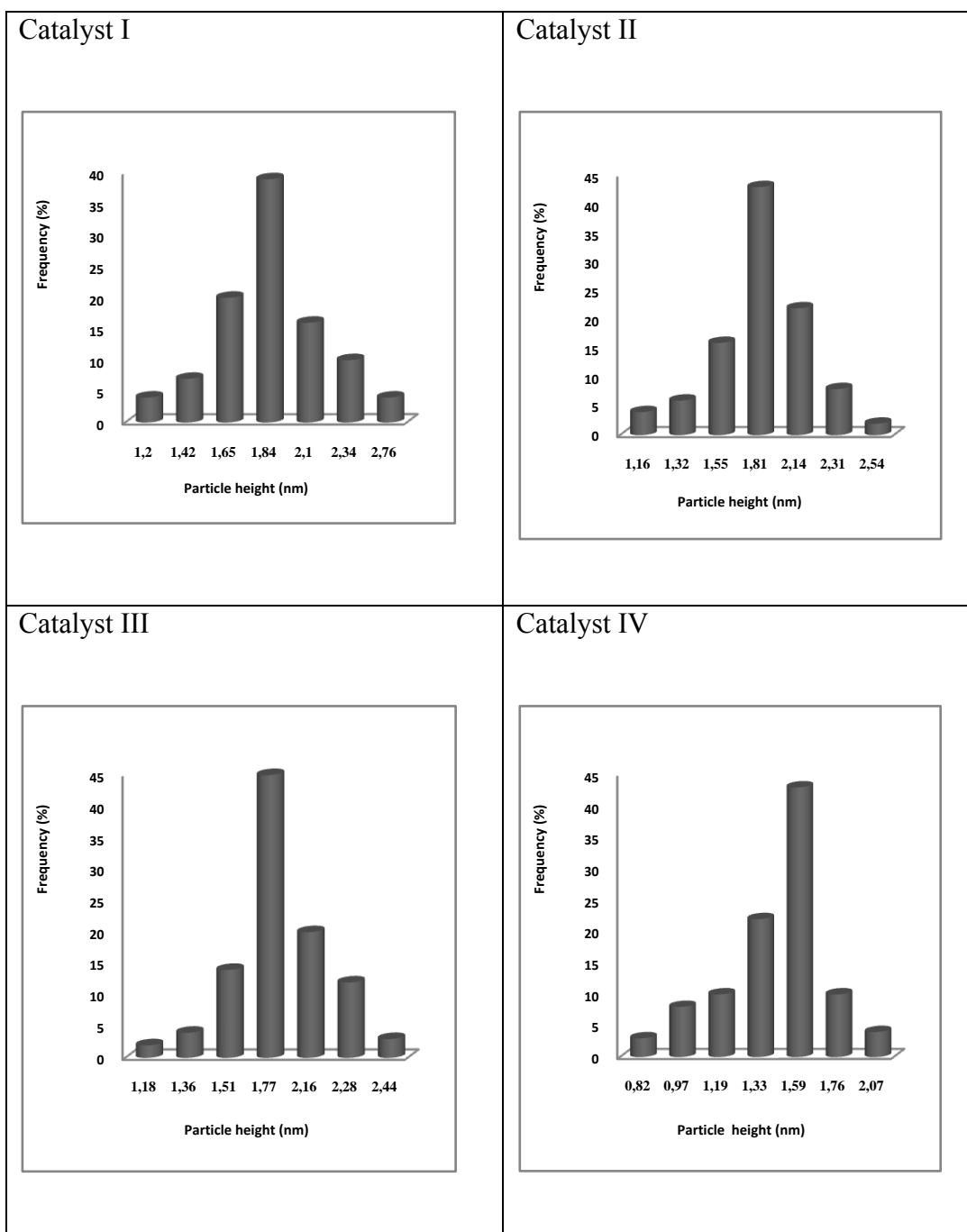


**Figure 3.6.** Histogram of height of particles obtained from AFM data.

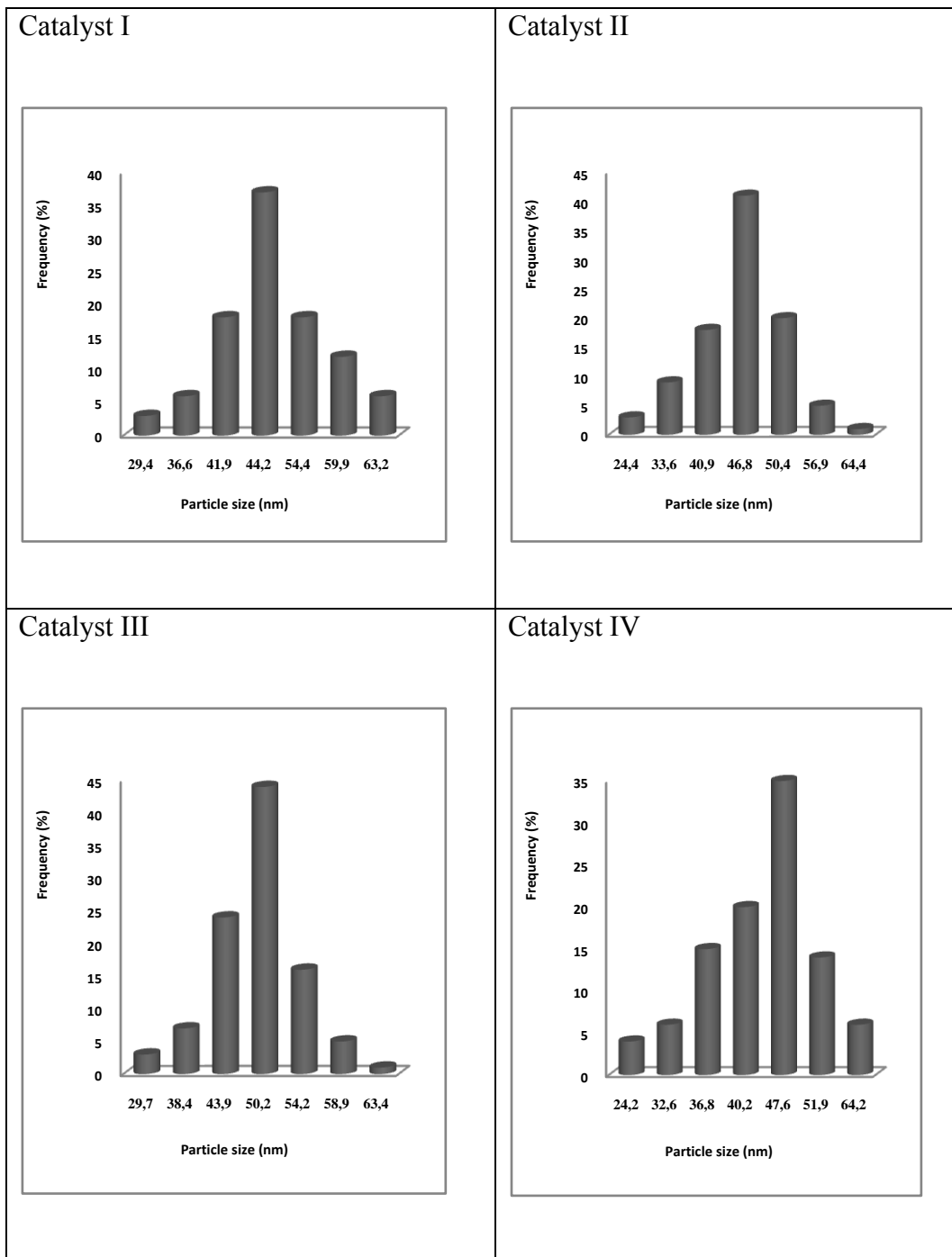


**Figure 3.7.** Histogram of lateral diameters of particles obtained from AFM data.

### 3.4. CYCLIC VOLTAMMETRY

Cyclic voltammograms of all carbon supported prepared catalysts were recorded in 0.1 M HClO<sub>4</sub> at room temperature with a scan rate of 50 mV/s and a typical representative voltammogram is given in Fig.3.8. Hydrogen adsorption/desorption regions were observed at -0.4 V and oxygen adsorption/desorption regions were observed at about 0.8 V and 0.4 V, respectively. A drastic change is recorded in the cyclic voltammograms due to the addition of methanol to acid solution. The similar changes were also observed in the cyclic voltammograms in the case of addition of ethanol and 2-propanol.

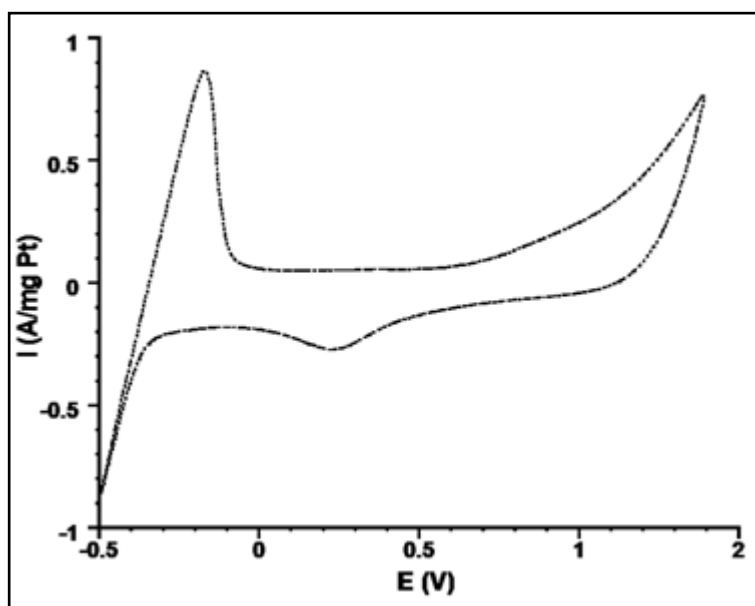


**Figure 3.8.** Cyclic voltammogram of catalyst I in 0.1 M HClO<sub>4</sub> at room temperature. Scan rate is 50 mV/s.

The electro-oxidation of methanol on Pt nanoparticles was characterized by two well-defined current peaks on the forward and reverse scans, Figure 3.9. In the forward scan, the oxidation peak is corresponding to the oxidation of freshly chemisorbed species which come from methanol adsorption. The reverse scan peak

is primarily associated with removal of carbonaceous species which are not completely oxidized in the forward scan. The magnitude of the peak current on the forward scan indicates the activity of the catalysts for the electro-oxidation reaction of alcohol.

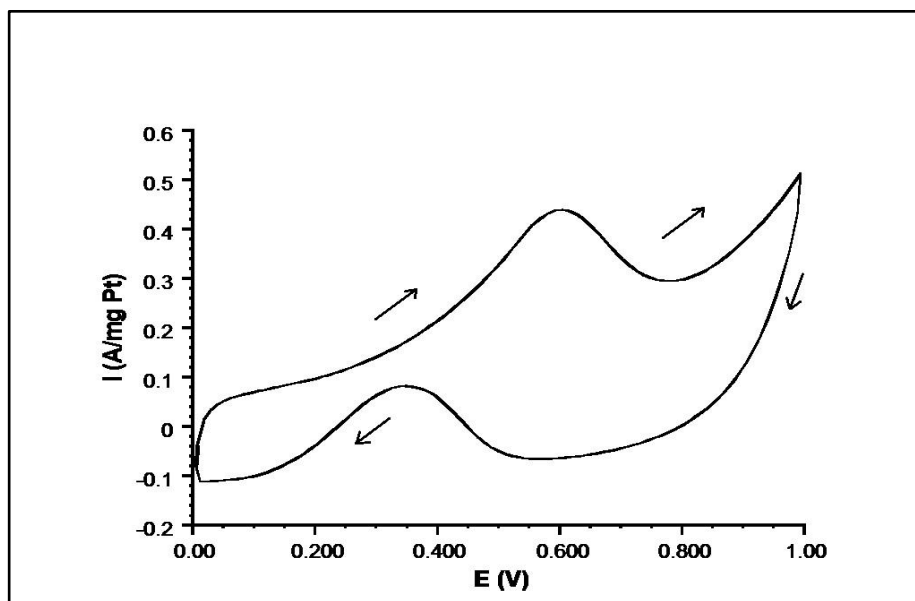


**Figure 3.9.** Cyclic voltammogram of catalyst I in 0.1 M HClO<sub>4</sub> and MeOH at room temperature. Scan rate is 50 mV/s.

The anodic parts of the cyclic voltammogram for all prepared catalysts showed that catalyst I had the maximum activity ( $\sim 0.44$  A / mg Pt at 0.66 V for methanol,  $\sim 0.28$  A / mg Pt at 0.58 V for ethanol and 0.74 A/mg Pt at 0.52 V for 2-propanol) compared to the others as shown in Figures 3.10., 3.11., 3.12., respectively. Enhancement in the activity of this catalyst compared to commercially available Pt ones is about 5.9, 11.0 and 9.9 times for methanol, ethanol and 2-propanol oxidation reactions, respectively and the catalytic activities onset and anodic potentials of all prepared catalysts were summarized in Table 3.6. Considering the electrochemical studies, it was possible to say that catalyst I had the highest catalytic activity towards alcohol oxidation reaction.

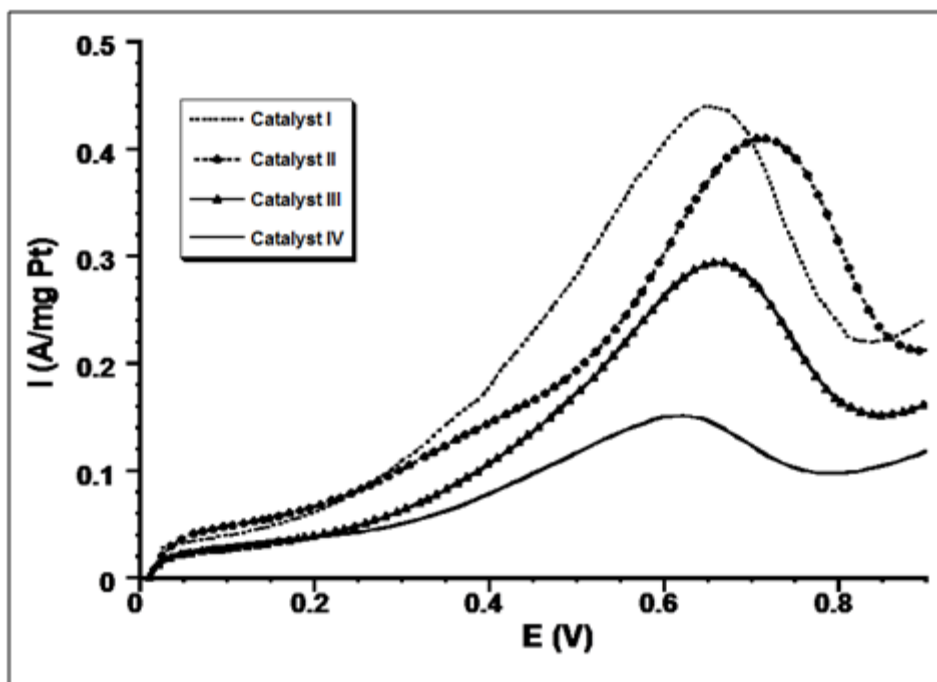


**Figure 3.10.** Anodic part of the cyclic voltammogram of catalysts in 0.1 M HClO<sub>4</sub> + 0.5 M CH<sub>3</sub>OH at room temperature. Scan rate is 50 mV/s.

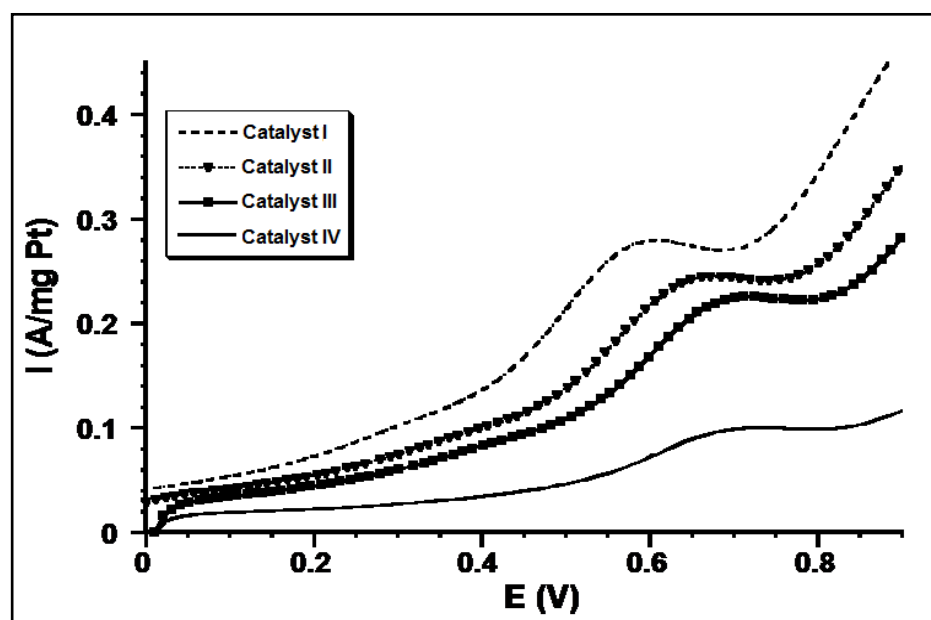


**Figure 3.11.** Anodic part of the cyclic voltammogram of catalysts in 0.1 M HClO<sub>4</sub> + 0.5 M CH<sub>3</sub>CH<sub>2</sub>OH at room temperature. Scan rate is 50 mV/s.

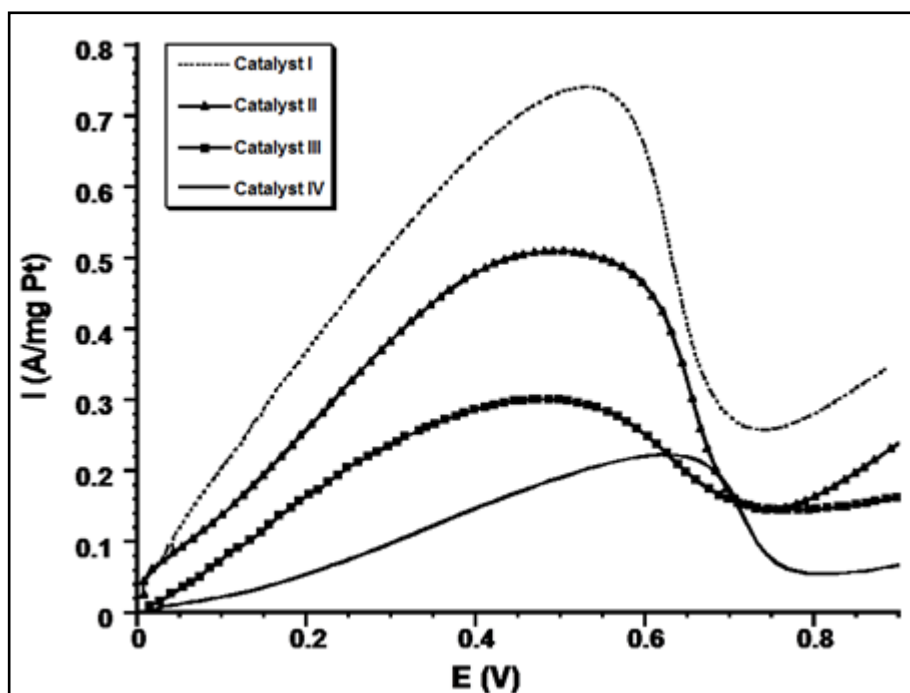


**Figure 3.12.** Anodic part of the cyclic voltammogram of catalysts in 0.1 M HClO<sub>4</sub> + 0.5 M 2-propanol at room temperature. Scan rate is 50 mV/s.

Table 3.6. also shows the  $I_f/I_b$  ratios where  $I_f$  is the current in the forward scan and  $I_b$  is the current in the reverse scan for all prepared catalysts in MeOH, EtOH and 2-propanol and these ratios indicate the performance of the catalysts. High  $I_f/I_b$  ratio indicates good alcohol oxidation to final product during anodic scan and low accumulation of intermediate species on the surface of catalysts<sup>41, 42</sup>. Catalyst I has highest  $I_f/I_b$  ratios which indicates the low poisoning of catalyst surface during alcohol oxidation.

**Table 3.6.** Maximum currents, onset and anodic peak potentials and  $I_f/I_b$  ratios for all catalysts in MeOH, EtOH and 2-propanol.

		<b>Catalyst I</b>	<b>Catalyst II</b>	<b>Catalyst III</b>	<b>Catalyst IV</b>
<b>In MeOH</b>	Max Current (A/mg Pt)	0.44	0.41	0.29	0.14
	Peak Position at Maximum Current (V)	0.66	0.71	0.68	0.62
	Onset (V)	0.24	0.26	0.27	0.30
	$I_f/I_b$	5.20	1.32	3.16	2.30
<b>In EtOH</b>	Max Current (A/mg Pt)	0.28	0.24	0.23	0.11
	Peak Position at Maximum Current (V)	0.58	0.62	0.67	0.68
	Onset (V)	0.45	0.47	0.51	0.55
	$I_f/I_b$	9.30	1.25	7.71	2.19
<b>In 2- propanol</b>	Max Current (A/mg Pt)	0.74	0.50	0.28	0.23
	Peak Position at Maximum Current (V)	0.53	0.54	0.50	0.66
	Onset (V)	0.03	0.06	0.04	0.15
	$I_f/I_b$	1.56	1.09	1.46	1.42

Besides, the electrochemical performances of the oxidation reaction of methanol, ethanol and 2-propanol can be compared to catalyst I. It is clear that the current densities of 2-propanol oxidation at corresponding potentials are higher than that of methanol and ethanol oxidation on our catalysts. For instance, the maximum current

density of 2-propanol oxidation is about 1.68 and 2.64 times better than that of methanol, ethanol on catalyst I, respectively. The activity order of alcohol oxidation on our catalysts is 2-propanol > methanol > ethanol. This can be explained by lower reaction rate of the intermediate formation for 2-propanol than that of methanol. This suggest a direct reaction path from 2-propanol to acetone, which does not go through an intermediate. As a result of this, it shows lower overpotential and higher performance than methanol<sup>43</sup>. Besides, 2-propanol has very low onset potential compared to other alcohols (Table 3.6.). This means that, in a low potential region, the overall oxidation rate of 2-propanol was higher than methanol. For example, the onset potential order of alcohol oxidation is 2-propanol (0.03 V) < methanol (0.24 V) < ethanol (0.45 V) for catalysts I.

In order to find the percent Pt utilities of the catalysts, the values of the electrochemical surface area (ECSA), which represents the active points on the surface of the catalysts towards electro-oxidation of alcohols, and chemical surface area (CSA), which is the direct surface area calculated from particle size, are needed. ECSA of the catalyst were calculated from the Coulombic charge of the hydrogen desorption in the cyclic voltammograms and was obtained from the following formula<sup>44</sup>:

$$ECSA = \frac{Q \text{ (mC)}}{0.21 \text{ mC/cm}^2}$$

where Q is the electric charge for hydrogen desorption and 0.21 mC/cm<sup>2</sup> represents the charge required to oxidize a monolayer of H<sub>2</sub> on platinum. The chemical surface areas (CSA) of these nanocatalysts were calculated using following equation<sup>45</sup>,

$$CSA = \frac{6 \times 10^4}{\rho \times d}$$

where d is the mean Pt crystalline size in Å (from the XRD results) and ρ is the density of Pt metal (21.4 g/cm<sup>3</sup>). From these two areas (ECSA and CSA), it is possible to calculate the Pt utilization efficiency (%) using;

$$\text{Utilization} = \frac{ECSA}{CSA}$$

CSA, ECSA and Pt utility values were listed in Table 3.7. for catalyst I, II, III and IV. It was concluded that catalyst I had the highest active surface area compared to others which could be beneficial to higher catalytic activity. Moreover, these results showed that there is a significant increase in Pt utilization efficiency on catalyst I compared to the other prepared catalysts.

**Table 3.7.** The comparison of particle size, ECSA/CSA (%Pt utility) for all catalyst.

	<b>Particle Size (nm)</b>	<b>CSA (m<sup>2</sup>/g)</b>	<b>ECSA (m<sup>2</sup>/g)</b>	<b>(ECSA/CSA)*100 (% Pt utility)</b>
<b>Catalyst I</b>	~ 1.92	146.0	116.1	79.5
<b>Catalyst II</b>	~ 1.91	146.8	111.4	75.9
<b>Catalyst III</b>	~ 1.87	149.9	99.9	66.6
<b>Catalyst IV</b>	~ 1.28	219.0	80.6	36.8

It is believed that in order to explain these results following parameters should be taken into account: a) Pt (0) to Pt (IV) ratio, b) ECSA, c) % Pt utility and d) adsorbed species on the surface of platinum species. For active catalysts, if the catalyst is clean enough meaning that all of the surfactants and any other reactants are removed from catalyst, Pt (0) / Pt (IV) ratio is increased and resulting in higher ECSA, % Pt utility then as a consequence, catalytic activity will be increased. Moreover, the role of the adsorbed species (water and/or hydroxide) in the mechanism of this alcohol oxidation reaction is not fully understood at the moment. Our experimental results indicated that an increase in the amount of adsorbed H<sub>2</sub>O on the surface of catalysts caused an increase in the rate of oxidation of alcohol to higher oxidation state compounds. Concerning those parameters, Catalyst I had the highest Pt (0) to Pt (IV) ratio (8.17), ECSA (116.1), % Pt utility (% 79.5) and adsorbed water (% 28.6) compared to the others. From the XRD results it can be also stated that catalyst I had a clear pattern. Therefore, catalysts I had more catalytic activity compared to the other catalysts.

### 3.5. CHRONOAMPEROMETRY

The stability of all prepared catalysts was investigated by chronoamperometric (CA) techniques. For this purpose, CA curves for methanol, ethanol and 2-propanol oxidation on all prepared catalysts were measured and the curves for methanol oxidation are shown in Figure 3.13. at the potential 0.6 V (versus SCE) during 3600 s as an example. All the prepared Pt catalysts were applied on the electrodes with the same procedure used in cyclic voltammetry experiments. Chronoamperometry experiments are carried out in 0.1 M HClO<sub>4</sub> + 0.5 M C<sub>n</sub>H<sub>2n+1</sub>OH (n=1, 2, 3) at room temperature. As a result, at the end of the CA, the oxidation current is larger on catalyst I than those on catalysts II, III and IV after a decay of 3600 s. The more stable and poisoning-tolerance catalyst order is catalyst I > II > III > IV towards methanol, ethanol and 2-propanol oxidation. This result is in good agreement with those of the cyclic voltammograms measurements.

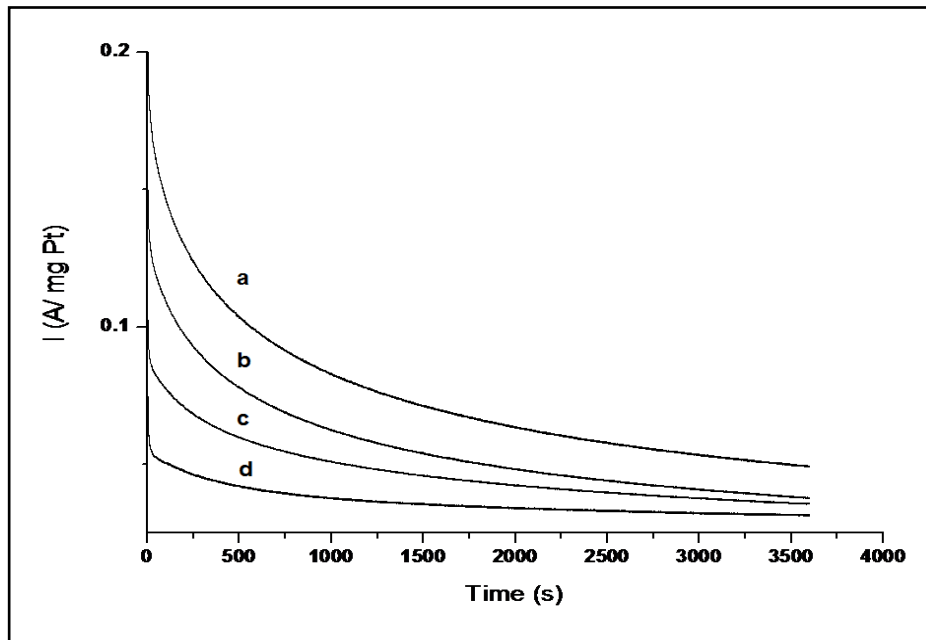


**Figure 3.13.** Chronoamperometric curves of methanol oxidation on catalyst I (a), II (b), III (c) and IV (d) at 0.6 V (vs. SCE) in 0.1 M HClO<sub>4</sub> + 0.5 M CH<sub>3</sub>OH.

## CHAPTER 4

### CONCLUSIONS

In this thesis, carbon supported Pt nanoparticles were prepared by using different surfactants, 1-octanethiol, 1-decanethiol, 1-dodecanethiol and 1-hexadecanethiol, analyzed, and employed for methanol, ethanol and 2-propanol oxidation reactions. The main results can be summarized as;

- It has been found that the structure of surfactant has an effect on the final size and correspondingly catalytic activities of metal nanoparticles. It can be stated that increase in chain length of the surfactants decreases the particle sizes of the catalysts. This was confirmed by AFM, XRD crystalline size and TEM results.
- The most active catalyst is found to be catalyst I. It is 5.9, 11.0 and 9.9 times more active compared to the commercial Pt catalyst for methanol, ethanol and 2-propanol oxidation reactions, respectively. The reason could be an increase in the ECSA, CO-tolerance, Pt (0) to Pt (IV) ratio, % Pt utility and Pt/S ratios.
- The decrease in the ratio of bounded to unbounded sulfur in thiolate species cause to increase the performance of the catalyst towards oxidation of reaction of alcohol.
- Adsorption of water instead of hydroxide on the surface of platinum nanoparticles increases the catalytic activity in the alcohol oxidation reaction.

- 2-Propanol electro-oxidation has higher activity on prepared catalysts than that of methanol and ethanol electro-oxidation. For instance, the maximum current density of 2-propanol oxidation is about 1.68 and 2.64 times better than that of methanol and ethanol on catalyst I, respectively due to lower reaction rate of the intermediate for 2-propanol. Besides, the onset potential of 2-propanol oxidation is lower than that of methanol and ethanol due to the higher overall oxidation rate of 2-propanol in a low potential range.

## REFERENCES

- <sup>1</sup> Kutz, M. , *Environmentaly Consious Alternatinve Energy Production*, John Wiley & Sons, Inc, New Jersey, 2007.
- <sup>2</sup> Online class notes for a course at Stanford Univesity  
<http://www.stanford.edu/class/e297a/Past,%20Present%20and%20Future%20of%20Petroleum.pdf>, August 3, 2011.
- <sup>3</sup> Zhao, T.S., Kreuer, K.D., Van Enguyen, T., *Advances in Fuel Cell Tecnology*, Elsevier Ltd., Vol. 1, Oxford, UK, 2007.
- <sup>4</sup> Hoogers, G., Section I, *Fuel Cell Technology Handbook*, CRS Press LLC, Florida, 2003.
- <sup>5</sup> Basu, S., *Recent Trends in Fuel Cell Science and Technology*, Anamaya Publishers, India, 2007.
- <sup>6</sup> Bagotsky, V.S., *Fuel Cells: Problems and Solutions*, John Wiley & Sons, Inc., New Jersey, 2009.
- <sup>7</sup> Srinivasan, S., *Fuel Cells; From Fundamental to Applications*, Springer, USA, 2006.
- <sup>8</sup> U.S. Department of Energy Hydrogen Programs; [www.hydrogen.energy.gov](http://www.hydrogen.energy.gov).
- <sup>9</sup> Sammes, N., *Fuel Cell Technology; Reaching Towards Commercialization*, Springer, Germany, 2006.
- <sup>10</sup> Gupta, S.S., Datta, J., *J. Chem. Sci.*, 117, 4, 337-344, 2005.
- <sup>11</sup> Arun Kumar, J., Kalyani, P., Saravanan, R., *Int. J. Electrochem. Sci.*, 3, 961-969, 2008.
- <sup>12</sup> Qian, W., Wilkinson, D.P., Shen, J., Wang, H., Zhang, J., *Journal of Power Source*, 154, 202-213, 2006.
- <sup>13</sup> D. Cao, S.H. Bergens, *J. Power Sources* 124, 12–17, 2003.
- <sup>14</sup> Hosokawa, M., Nogi, K., Naito, M., Yokoyama, T., *Nanoparticle Technology Handbook*, 1st Ed., Elsevier, The Netherlands, 2007.
- <sup>15</sup> Roucoux, A., Schulz, J., Patin, H., *Chem. Rev.*, 102, 3757-78, 2002.

- <sup>16</sup> Wiki service of North Caroline State University,  
<http://wikis.lib.ncsu.edu/index.php/Nanoparticles>, May 4, 2008.
- <sup>17</sup> University of Washington Departments Web Server,  
[http://depts.washington.edu/solgel/images/courses/MSE\\_502/Ch\\_2/figure\\_2.22.JPG](http://depts.washington.edu/solgel/images/courses/MSE_502/Ch_2/figure_2.22.JPG) ,  
October 5, 2005.
- <sup>18</sup> Şen, F., Gökağaç, G., *J. Phys. Chem. C*, 111, 15, 5715-20, 2007.
- <sup>19</sup> Yee, C., Scotti, M., Ulman, A., White, H., Rafailovich, M., Sokolov, J., *Langmuir*,  
15, 4314-16, 1995.
- <sup>20</sup> Şen, S., *Activity of Carbon Supported Platinum Nanoparticles Toward Methanol  
Oxidation Reactions: Role of Metal Precursor and New Surfactants*, METU, Ankara,  
2008.
- <sup>21</sup> (JCPDS-ICDD, Card No. 04-802).
- <sup>22</sup> Klug, H.; Alexander, L., *X-ray diffraction procedures*, first ed., Wiley, New York,  
1954.
- <sup>23</sup> Mizukoshi, Y., Takagi E., Okuno, H., Oshima, R., Maeda, Y., Nagata, Y.,  
*Ultrasonics Sonochemistry*, 8, 1-6, 2001.
- <sup>24</sup> Kawasaki, H., Uota, M., Yoshimura, T., Fujikawa, D., Sakai, G., Kijima, T., *J.  
Coll. Inter. Sci.*, 300, 149-154, 2006.
- <sup>25</sup> Prabhuram, J., Wang, X., Hui, C.L., Hsing, I-M., *J. Phys. Chem. B*, 107, 11057-64,  
2003.
- <sup>26</sup> Colmati, F., Antolini, E., Gonzalez, E.R., *J. Power Sour.*, 157, 98-103, 2006.
- <sup>27</sup> Şen, F., Gökağaç, G., *J. Phys. Chem. C*, 111, 1467-73, 2007.
- <sup>28</sup> Yonezawa, T., Toshima, N., Wakai, C., Nakahara, M., Nishinaka, M., Tominaga,  
T., Nomura, H., *Coll. and Surf. A*, 169, 35-45, 2000.
- <sup>29</sup> Liang, L., Sun, G., Sun, S., Liu, J., Tang, S., Li, H., Zhou, B., Xin, Q.,  
*Electrochimica Acta*, 50, 5384-89, 2005.
- <sup>30</sup> Gökağaç, G., Kennedy, B.J., Cashion, J.D., Brown, L.J., *J. Chem. Soc. Faraday  
Trans.*, 89, 151-157, 1993.
- <sup>31</sup> Watanabe, M., Uchida, M., Motoo, S., *J. Electroanal. Chem.*, 229, 395-406, 1987.
- <sup>32</sup> Goodenough, J.B., Hamnett, A., Kennedy, B.J., Manoharan, R., Weeks, S.A., *J.  
Electroanal. Chem.*, 240, 133-145, 1988.

- <sup>33</sup> Jimenez, J.A., Liu, H., Fachini, E., *Materials Letters*, 64, 2046-48, 2010.
- <sup>34</sup> DiCenzo, S.B., Berry, S.D., Hartford, Jr., E.H., *Physical Review B*, 38, 8465-68, 1988.
- <sup>35</sup> Peuckert, M., *Electrochimica Acta*, 29, 10, 1315-1320, 1984.
- <sup>36</sup> Peuckert, M., Bonzel, H.P., *Surface Science*, 145, 1, 239-259, 1984.
- <sup>37</sup> Castner, D.G., Hinds, K., Grainger, D.W., *Langmuir*, 12, 5083-86, 1996.
- <sup>38</sup> Zubraegel, Ch., Deuper, C., Schneider, F., Neumann, M., Grunze, M., Schertel, A., Wöll, Ch., *Chemical Physics Letters*, 238 (4-6), 308-312, 1995.
- <sup>39</sup> Liu, Z., Yu, C., Russakova, I.A., Huang, D., Strasser, P., *Top Catal.*, 49, 241-250, 2008.
- <sup>40</sup> Raşa, M., Kuipers, B.W.M., Philipse, A.P., *J. Coll. Inter. Sci.*, 250, 303-315, 2002.
- <sup>41</sup> Liu, Z., Yi Ling, X., Su, X., Lee, J.Y., *J. Phys. Chem. B*, 108, 8234-40, 2004.
- <sup>42</sup> Gu, Y.J., Wong, W.T., *Langmuir*, 22, 11447-52, 2006.
- <sup>43</sup> Otomo, J., Li, X., Kobayashi, T., Wen, C-J., Nagamoto, H., Takahashi, H., *J. Electroanal. Chem.*, 573, 99-109, 2004.
- <sup>44</sup> Woods, R.J., *Electroanalytical Chemistry*, Marcel Dekker, Vol. 9, New York, 1-162, 1976.
- <sup>45</sup> Wang, Z.B., Yin, G.P., Shi, P.F., *J. Electrochem. Soc.*, 152, A2406-12, 2005.